Informes Técnicos Ciemat

1261

Octubre, 2012

Gas and Water Permeability of Concrete

M. V. Villar
P. L. Martín
F. J. Romero
V. Gutiérrez-Rodrigo
J. M. Barcala

GOBIERNO DE ESPAÑA

MINISTERIO DE ECONOMÍA Y COMPETITIVIDAD

Ciemat
Centro de Investigaciones Energéticas, Medioambientales y Tecnológicas

Informes Técnicos Ciemat

1261
Octubre, 2012

Gas and Water Permeability of Concrete

M. V. Villar
P. L. Martín
F. J. Romero
V. Gutiérrez- Rodrigo
J. M. Barcala

Departamento de Medio Ambiente

Toda correspondencia en relación con este trabajo debe dirigirse al Servicio de Información y Documentación, Centro de Investigaciones Energéticas, Medioambientales y Tecnológicas, Ciudad Universitaria, 28040-MADRID, ESPAÑA.

Las solicitudes de ejemplares deben dirigirse a este mismo Servicio.

Los descriptores se han seleccionado del Thesauro del DOE para describir las materias que contiene este informe con vistas a su recuperación. La catalogación se ha hecho utilizando el documento DOE/TIC-4602 (Rev. 1) Descriptive Cataloguing On-Line, y la clasificación de acuerdo con el documento DOE/TIC.4584-R7 Subject Categories and Scope publicados por el Office of Scientific and Technical Information del Departamento de Energía de los Estados Unidos.

Catálogo general de publicaciones oficiales
http://www.060.es

Depósito Legal: M -26385-2011
ISSN: 1135 - 9420
NIPO: 721-12-042-3

Editorial CIEMAT

CLASIFICACIÓN DOE Y DESCRIPTORES

S58
WATER; PERMEABILITY; CONCRETES; GASES; MEASURING METHODS;
PRESSURE EFFECTS

Gas and Water Permeability of Concrete

Villar, M. V.; Martín, P. L.; Romero, F. J.; Gutiérrez- Rodrigo, V.; Barcala, J. M.
45 pp. 14 ref. 37 figs. 21 tables

Abstract:
The gas pressure of concrete samples was measured in an unsteady-state equipment working under low injection pressures and in a newly fine tuned steady-state setup working under different pressures. These measurements allowed the estimation of the intrinsic and relative gas permeability of the concrete and of the effect of boundary conditions on them.
Permeability decreased with water content, but it was also greatly affected by the hydraulic history of concrete, i.e. if it had been previously dried or wetted. In particular, and for a given degree of saturation, the gas permeability of concrete previously saturated was lower than if the concrete had been just air dried or saturated after air drying. In any case, the gas permeability was about two orders of magnitude higher than the liquid water permeability (10-16 vs. 10-18 m2), probably due to the chemical reactions taking place during saturation (carbonation). The relative gas permeability of concrete increased sharply for water degrees of saturation smaller than 50%.
The boundary conditions also affected the gas permeability, which seemed to be mostly conditioned by the backpressure and the confining pressure, increasing as the former increased and decreasing as the latter increased, i.e. decreasing as the effective pressure increased. Overall the increase of pressure head or injection pressure implied a decrease in gas permeability. External,microcracking during air-drying could not be ruled out as responsible for the decrease of permeability with confining pressure.
The apparent permeability obtained applying the Klinkenberg method for a given effective pressure was only slightly smaller than the average of all the values measured for the same confining pressure range. For this reason it is considered that the Klinkenberg effect was not relevant in the range of pressures applied.

Permeabilidad al Gas y al Agua del Hormigón

Villar, M. V.; Martín, P. L.; Romero, F. J.; Gutiérrez- Rodrigo, V.; Barcala, J. M.
45 pp. 14 ref. 37 figs. 21 tablas

Resumen:
Se ha medido la permeabilidad al gas de muestras de hormigón en un equipo de carga variable en el que se aplican presiones bajas y en un equipo de carga fija, puesto a punto para este proyecto, en el que se aplican presiones más altas. Con estas medidas se han estimado la permeabilidad intrínseca y relativa del hormigón y el efecto de las condiciones de contorno sobre ellas.
La permeabilidad al gas disminuye con la humedad, pero también depende de la historia hidráulica del hormigón. En concreto, para un grado de saturación dado la permeabilidad del hormigón previamente saturado es más baja que la de éste sólo secado al aire o saturado después de haber sido secado al aire. La permeabilidad al gas es dos órdenes de magnitud inferior que la permeabilidad saturada al agua (10-16 vs. 10-18 m2), probablemente debido a las reacciones químicas que se producen durante la saturación (carbonatación). La permeabilidad relativa al gas aumenta significativamente para grados de saturación en agua inferiores al 50%.
La permeabilidad al gas también se ve afectada por las condiciones de contorno, en particular por la presión de cola, con la que aumenta, y la confinante, con la que disminuye, es decir, en general disminuye al aumentar la presión efectiva. Normalmente, al aumentar la carga hidráulica o la presión de inyección la permeabilidad disminuye. La microfracturación superficial durante el secado no puede descartarse como responsable de la disminución de la permeabilidad con la presión confinante.
La permeabilidad aparente obtenida mediante el método Klinkenberg para una presión efectiva dada es sólo algo inferior a la media de todos los valores medidos para el mismo rango de presiones confinantes, por lo que se considera que el efecto Klinkenberg no es relevante en el rango de presiones aplicadas.

Contents

1 Introduction

In most countries the final disposal of low and intermediate-level radioactive waste is performed on surface or near-surface facilities, in which concrete is frequently used as a barrier. This work is a contribution to the understanding of the behaviour of concrete barriers in surface disposal facilities, in particular in the Spanish disposal facility of El Cabril, where the waste containers are placed inside concrete cells. The durability of concrete and its mechanical properties are intrinsically bound to moisture transport effects, especially when it is subjected to repeated wetting and drying regimes, and that is why a detailed thermo-hydraulic characterisation is necessary to model its behaviour.

Thus, with a view on LLW and ILW issues, gas permeability measurements were performed in concrete samples of different degrees of saturation under low gas pressure and gradient (<0.1 MPa) in an unsteady-state equipment and under variable confining, injection and backpressures (in the range 0.1-1.6 MPa) in a steady-state permeameter. In addition, the saturated hydraulic conductivity of the same samples was measured after saturating them with water as percolating fluid. This work was carried out by CIEMAT in FORGE WP3.4.3 "Concrete laboratory experiments".

2 Material

The concrete used was manufactured at the C.A. El Cabril in September 2006 and May 2008 in the form of cylindrical blocks casted in PVC molds of different sizes, following the procedures used to manufacture the disposal cells. The samples were cured at El Cabril at ambient temperature, and once at CIEMAT they were kept in a high-RH atmosphere (wet chamber) and at room temperature (Villar *et al*. 2009). The concrete had a characteristic strength of 350 kp/cm^2, with a water/cement ratio of 0.43 and a consistency of 14 cm. Its average pore size was 0.03 µm (Zuloaga 2008). The specific weight of solid particles of the concrete was 2.68. The concrete theoretical composition, which included OPC, was the following:

aggregates 4/16	41.9%
sand 0/4	26.0%
sand 0/2	8.3%
cement I 42,5R/SR	16.4%
Melcret-222 additive	0.3%
water	7.2%

The pore size distribution of the concrete was obtained by mercury intrusion porosimetry in some lyophilised fragments (Figure 1). The percentage of pores of diameter smaller of 2 nm (micropores) was 39±7 and of those larger than 50 nm (macropores) was 49±5. The pore mode was around 92±13 nm, and the porosity about 10 percent.

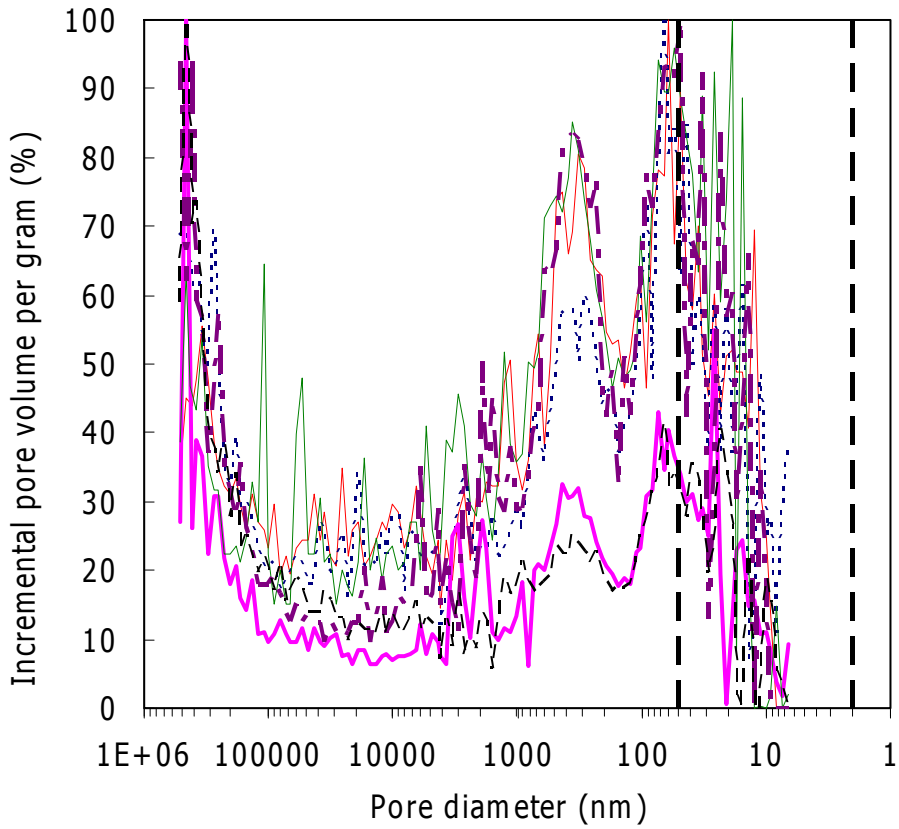

Figure 1: Pore size distribution obtained by mercury intrusion porosimetry in lyophilised concrete samples

3 Methodology

The cylindrical concrete samples casted at El Cabril were kept in CIEMAT inside a "wet chamber". When needed the samples were cut to fit the cell dimensions and to obtain perfectly parallel surfaces on top and bottom. The specimens thus prepared had diameters of 35 or 50 mm and heights between 40 and 70 mm. These samples were allowed to air dry and their gas permeability was measured in several moments along the drying process, hence the gas permeability was obtained for different concrete water contents. The same samples were also water saturated to determine in them the hydraulic conductivity and then allowed to air dry again, measuring the gas permeability at different moments during this second drying process. Some of these samples were water saturated for a second time and among them some were air dried for a third time. The aim of this testing procedure was to check the impact of hydraulic history on permeability. A total of 10 cylindrical samples were used, whose dimensions, dry density (ρ_d) and porosity (n) are given in Table I. The average dry density value was 2.31±0.04 g/cm^3, corresponding to a porosity of 13.7±1.5% and a void ratio of 0.16±0.02. The tests performed in them are summarised in Table II, in which the duration of the consecutive drying and wetting periods is indicated. The gas permeability tests had references starting by "PG" whereas the water permeability tests had references starting by "HOR".

At the end of each test, the concrete specimens were measured and weighed to estimate the water content and dry density, although the actual values could not be computed until all the different tests on a same sample were completed and the sample was dried at 110°C during 48 h to determine the dry mass.

Table I: Characteristics of the concrete samples used for the permeability tests

Sample	Height (cm)	Diameter (cm)	ρ_d (g/cm^3)	*n* (%)
0	4.7	3.5	2.26	16
1	6.8	5.0	2.37	12
2	5.6	5.0	2.32	14
3	6.2	5.0	2.36	12
4	6.9	3.5	2.32	14
5	4.1	3.5	2.32	13
6	5.4	3.5	2.31	14
7	5.4	3.5	2.30	14
9	5.1	3.5	2.32	13
10	5.2	5.0	2.24	16

Table II: Summary of tests performed on the concrete samples

Sample	Dry (days)	Tests	Wet (days)	Tests	Dry (days)	Tests	Wet (days)	Tests	Dry (days)	Tests
0			40	HOR0						
1	787	PG1_1 to 9	511	HOR1s	409	PG1_10 to 17	253	HOR1s_2		
2	511	PG2_1 to 7	19	HOR2s	273	PG2_8 to 11				
3	5		23	HOR3	958	PG3_1 to 8	254	HOR3s_2	368	PG3_9 to 18
4	1		19	HOR4	348	PG4_1	39	HOR4s	395	PG4_2 to 7
5	5		56	HOR5	255	PG5_1 to 5	28	HOR5s	270	PG5_6 to 8
			107	HOR5s_2	630	PG5_9 to 14				
6	179		58	HOR6s	628	PG6_1 to 2	169	HOR6s_2	601	PG6_3 to 6
			92	HOR6s_3						
7	259	PG7_1 to 3	179	HOR7s	308	PG7_4 to 8	333	HOR7s_2		
9	346	PG9_1 to 3	325	HOR9s	137	PG9_4 to 7				
10	601	PG10_1 to 10	190	HOR10s						

3.1 GAS PERMEABILITY

Two different experimental setups were used to determine the gas permeability, a steady and a unsteady-state one. The unsteady-state method had been used at CIEMAT for more than a decade, whereas the steady-state method was fine tuned for this project (Villar *et al*. 2010). The aim of the first kind of tests was to determine the influence of water content and degree of

saturation on gas permeability, whereas the aim of the tests performed on the steady-state permeameter was to analyse the effect of boundary conditions, such as gas pressure and confining pressure, on gas permeability.

It must be pointed out that no sample was completely dry (0% water content) during the determinations and therefore, the intrinsic permeability could not be directly obtained from the gas measurements performed, since to determine the intrinsic permeability with air flow the sample must be completely dry. In order to obtain completely dry samples it would have been necessary to dry them in the oven at 110°C and this would have caused changes in the microstructure of the concrete and consequently in its hydraulic properties. When there are two fluids present in the porous material (gas and water in this case), the permeabilities of each fluid depend upon the saturation of each fluid: these are called apparent (or effective) permeabilities. Hence, the value obtained in the determinations (apart from the gas permeability, k_g) is the intrinsic permeability measured with gas flow, k_{ig}, multiplied by the relative permeability to gas, k_{rg}. In turn, the relative permeability to gas is the ratio of the apparent permeability of gas at a particular saturation to the absolute permeability of gas at total gas saturation, *i.e*. in completely dry material, where the k_{rg} value would be 1.

3.1.1 Unsteady-state method

The cartoon of the assembly for the unsteady-stated determination is shown in Figure 2. The cylindrical concrete samples were placed in a triaxial cell confined between two porous stones and wrapped in two latex membranes, between which vacuum grease was applied in order to prevent the loss of gas. The cell walls were made of methacrylate and were capable of withstanding pressures of up to 3000 kPa (Figure 3). The cell had three inlets drilled in the base: for the sample top drainage/backpressure, for the sample bottom injection pressure, and for the confining pressure. A pressure was applied to the chamber of the triaxial cell, high enough to ensure perfect adherence of the latex membranes to the walls of the sample (this pressure may have an influence on the permeability value obtained, and was usually of 0.6 MPa). The inlet at the lower part of the sample was connected to an airtight tank of known volume, in which nitrogen gas was previously injected at a pressure slightly higher than atmospheric. The tank was instrumented with a pressure sensor, connected to a data acquisition system, which recorded the pressure of the fluid contained inside. The inlet at the upper part of the sample was left open to the atmosphere. The test consisted in allowing the air in the tank to go out to the atmosphere through the specimen, while the decrease in pressure in the tank was measured as a function of time. The tests were performed at constant, room temperature.

Prior to the permeability test, the airtightness of the system was checked for every new test.

The permeability to gas was calculated in accordance with the following equation (Yoshimi & Osterberg 1963):

$$k_g = 2.3 \times \frac{V \times L \times \rho_g \times g}{A \times \left(P_{atm} + P_0/4 \right)} \times \frac{-Log_{10}\left(P(t)/P_0 \right)}{t\text{-}t_0} \qquad [1]$$

where k_g is the permeability to gas (m/s), V the volume of the tank (m^3), L the length of the sample (m), A the surface area of the sample (m^2), ρ_g the density of the gas (kg/m^3), P_{atm} is atmospheric pressure (N/m^2), P_0 is the excess of pressure over atmospheric pressure in time t_0 (s) and $P(t)$ is the excess over atmospheric pressure in the tank in time t. This equation was developed in a way analogous to that used for the expression of permeability to water using a

falling head permeameter, with the air continuity equation being applied through consideration of compressibility (Lloret 1982). In developing the equation, it was assumed that the initial P_0 pressures are relatively small compared to atmospheric pressure. Also it must be assumed that while the pressure is decreasing in the tank, the distribution of pressure in the soil sample is the same as would exist if this instantaneous pressure had been maintained in the tank for a long period of time. The volume of the spherical tank used was $2.21 \cdot 10^{-2}$ m^3 and the gas used for the tests was nitrogen, for which a density of 1.12 kg/m^3 was taken. The pressure of the tank on test initiation was fixed at values close to 103 kPa, since keeping the properties of the gas constant throughout the test requires that it not be subjected to high pressures.

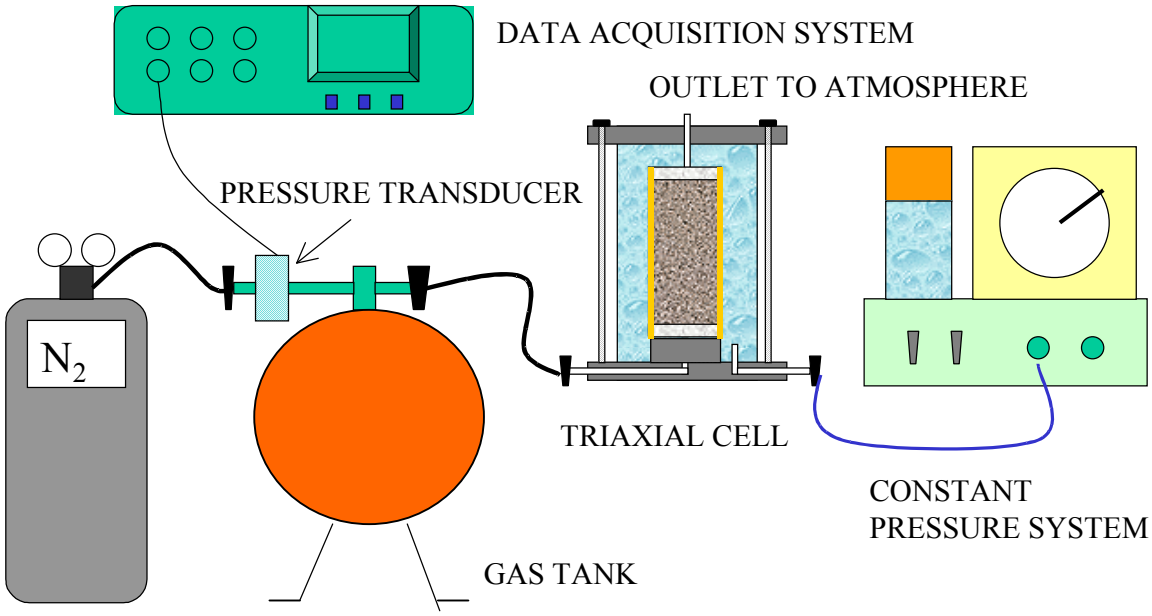

Figure 2: Schematic representation of the unsteady-state gas permeability system

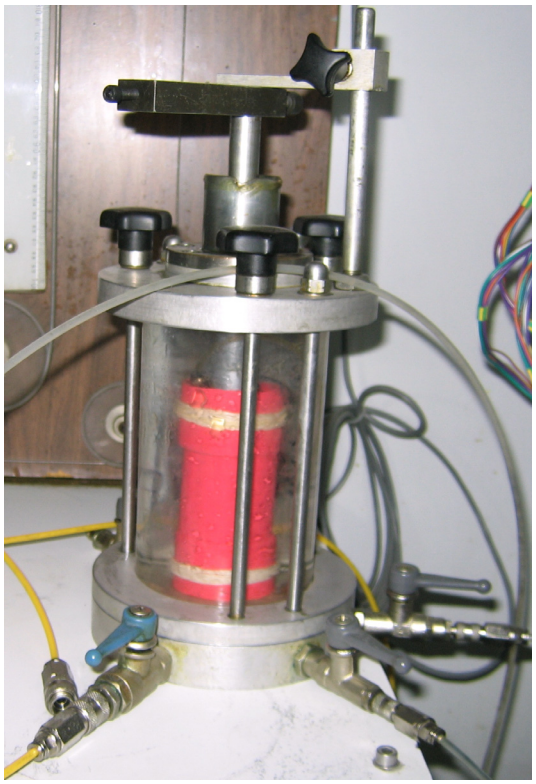

Figure 3: Concrete sample inside a methacrylate triaxial cell

Taking into account the dynamic viscosity of nitrogen (μ_g, $1.79 \cdot 10^{-5}$ Pa·s), the following relation between permeability to gas (k_g, m/s) and the product of intrinsic permeability measured with nitrogen gas (k_{ig}, m^2) times the relative permeability to gas (k_{rg}) is obtained:

$$k_g = \frac{\rho_g \times g}{\mu_g} \times k_{ig} \times k_{rg} = 6.2 \cdot 10^5 \times k_{ig} \times k_{rg} \quad [2]$$

3.1.2 Steady-state method

The concrete cylindrical samples were prepared and placed in a triaxial cell in the same way described in the previous section, the only difference being that the injection pressure in these tests was applied on top.

The setup to perform gas permeability measurements was designed to work as a constant head permeameter under different gas pressures, with the possibility to change the head value and measure the gas inflow and outflow (Figure 4). The triaxial cell was filled with water and pressurised with nitrogen, which was separated from the water in the cell through an elastic membrane contained in an OLAER's pressure accumulator. The injection and downstream pressures could be independently varied and kept constant during the period of time necessary to get steady flow by HI-TEC gas forward pressure controllers. Associated to the pressure controllers, DRUCK pressure transmitters (PTX1400 series, 100 bar a, 0.15% typical accuracy, overpressure 2 x FS), were placed for redundancy at the inlet and outlet of the cell. Different range HITECH gas mass flowmeters measured the inward and outward flows (0.2-10, 2-100 and 20-1000 STP cm^3/min). Gas mass flowmeters were used to prevent the potential impact of deviation from the ideal behaviour of gas on the measurement of the molecular flow rate and, hence, on the calculated permeability coefficients. Nitrogen gas was used as fluid. The technical details of the equipment were given in Villar *et al*. (2010).

The system applied the pressures to the sample and registered flow and pressures from the measurement devices. In and outflow gas rates, up and downstream pressure, temperatures and the confining pressure were monitored.

To compute the apparent (or effective) permeability (intrinsic permeability measured with gas flow, k_{ig}, relative permeability to gas, k_{rg}) the inflow or outflow measurements could be used, applying the following equation for incompressible media with compressible pore fluids (Scheidegger 1974):

$$k_{ig} \cdot k_{rg} = \frac{Q_m \times \mu_g \times L \times 2P_m}{A \times (P_{up}^2 - P_{dw}^2)} \quad [3]$$

where Q_m is the measured flow (volume of fluid as a function of time), A is the sample surface area, μ_g is the fluid dynamic viscosity, L is the sample length and P_{up} and P_{dw} are the upstream and downstream pressures applied at the top (inlet) and the bottom (outlet), respectively, of the sample, and P_m is the pressure of the measured flow (in our case, due to the STP conditions of the gas mass flowmeters, the atmospheric pressure). In turn gas permeability, k_g, could be computed taking into account the gas density and viscosity change with upstream or downstream pressures (P):

$$k_g = \frac{\rho_g \times g \times P}{\mu_g} \times k_{ig} \times k_{rg} \quad [4]$$

It was considered that the viscosity of nitrogen did not change during the tests because they were isothermal, whereas density changed with pressure. The change in density was considered as that of an ideal gas, and thus computed as the product of the density of nitrogen at atmospheric pressure times the pressure, either the injection or the backpressure, depending on what flow was used for the computation. This solution assumed that steady state flow was established, what meant that the quantity of gas exiting the sample in the low pressure side was equal to that entering the sample in the high pressure side. This aspect was verified in the tests. In any case, the underestimation of the calculated permeability coefficients should be less than 1.3%.

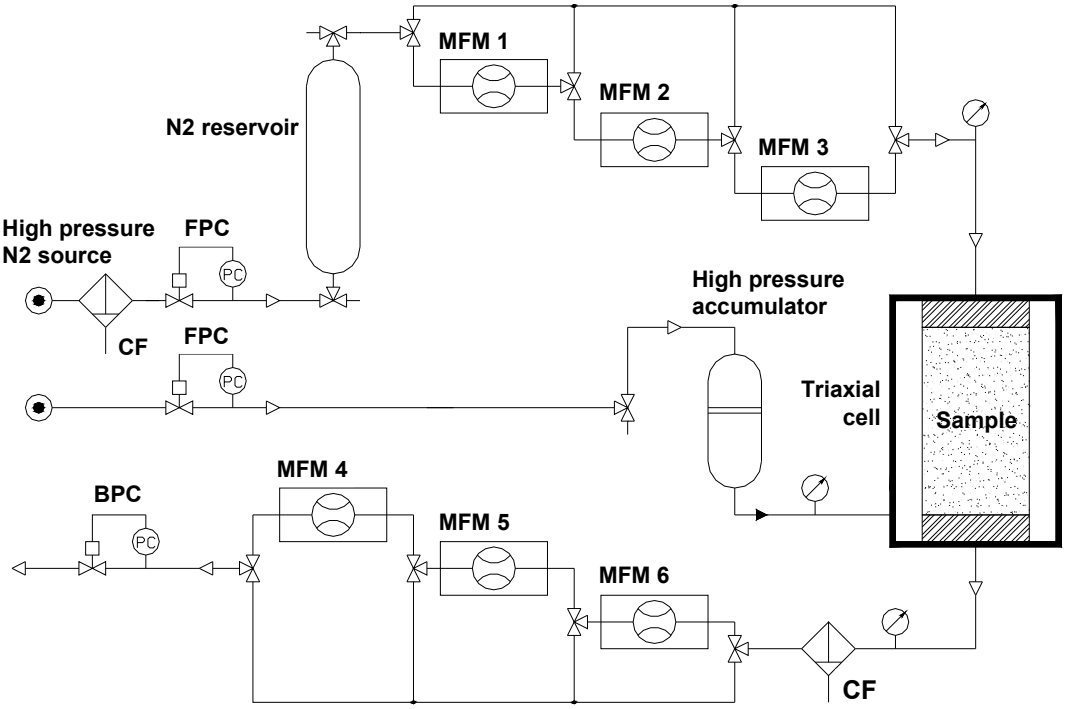

Figure 4: Schematic diagram of the setup for the steady-state gas permeability tests (CF: coalescing filter; FPC: forward pressure controller; BPC: back pressure controller; MFM: mass flowmeter (1000 mLn/min: 1&6; 100 mLn/min: 2&5; 10 mLn/min: 3&4); black arrow: water line for confining pressure)

3.2 WATER PERMEABILITY

The hydraulic conductivity of the saturated samples was measured in a constant head permeameter. Basically, the method consisted in measuring against time the volume of water crossing a saturated, laterally confined specimen to which a constant hydraulic gradient between the upper and lower ends was applied. Thus, the method consisted in applying a hydraulic head (ΔP) between the upper and lower ends of a sample of known dimensions (surface area: A, height: L) previously saturated. Simultaneously, the volume of water passing through the sample (ΔV) was determined over a given time period (Δt, s). Hydraulic conductivity (water permeability, k_w) was calculated by applying Darcy's law for flow in porous media:

$$k_w = \frac{\Delta V \times L}{A \times \Delta t \times \Delta P} \quad [5]$$

The intrinsic permeability (k_{iw}) was calculated from the water permeability determined in saturated samples through:

$$k_{iw} = \frac{k_w \times \mu_w}{\rho_w \times g} \quad [6]$$

where μ_w is the water dynamic viscosity (taken as $1 \cdot 10^{-3}$ Pa·s), ρ_w is the water density (taken as 1 kg/m^3) and g was taken as 9.8 m/s^2.

To perform the determination the samples were wrapped in a latex membrane, porous stones were placed on top and bottom and it was mounted in a triaxial cell. The cell was pressurised with water at 0.8-1.0 MPa and deionised water was injected through top and bottom of the sample at a pressure of 0.6 MPa in order to saturate it. Once saturated a nominal hydraulic head of 0.1 MPa was applied to the sample by increasing the injection pressure at its bottom in order to perform the flow measurement.

Due to the particular characteristics of the material, the permeability value changed over time. For this reason the measurements were repeated periodically over several months. Between measurements, the samples were kept saturating in the same triaxial cells. The determinations were done at laboratory temperature.

4 Results

4.1 GAS PERMEABILITY

4.1.1 Unsteady-state method

The aim of the first kind of tests was to determine the influence of concrete water content and degree of saturation on its gas permeability. To this point the same specimen was measured several times after taking it out of the wet chamber, letting it dry at laboratory conditions between the different measurements (Table II). In this way the change of gas permeability during drying was evaluated. The Tables in Appendix 1 summarise the results obtained for the measurements performed in each specimen, expressed as gas permeability (k_g) and as intrinsic permeability times relative permeability ($k_{ig} \cdot k_{rg}$). The effective degree of saturation is also included, $e(1\text{-}S_r)$, where e is the void ratio and S_r the water degree of saturation.

Most samples were initially air dried to determine the evolution of gas permeability with water content. The same samples were later water saturated to determine in them the saturated permeability and then let air-dry again while the gas permeability was measured The results obtained for these samples are shown in Figure 5, Figure 6 and Figure 7. Conversely, some specimens were first water saturated and the gas permeability was measured afterwards during air-drying, and later after a second water saturation and air-drying (Figure 8 and Figure 9). The figures show that the gas permeability increased with the water content diminution and that it was systematically lower (for the same water content) when the concrete had been previously saturated (up to an order of magnitude). The same trends were found when the intrinsic permeability values were considered. These values are shown in Figure 10 as a function of water content for all the samples tested. Gas permeability of concrete was between $1.6 \cdot 10^{-9}$ and $4.8 \cdot 10^{-12}$ m/s or between $1.8 \cdot 10^{-15}$ and $2.5 \cdot 10^{-18}$ m^2 if it is expressed as $k_{ig} \cdot k_{rg}$, for water contents between 0.5 and 4.3 %, corresponding to degrees of saturation between 9 and 86 %. Figure 11 shows the same results as a function of the time of drying. Of course, the longer the drying time the higher the gas permeability, because the water content decreased on drying,

but it appears that after approximately 300 days drying, the gas permeability did not change, probably because an equilibrium water content (Figure 12) and a chemical equilibrium with the atmosphere were reached.

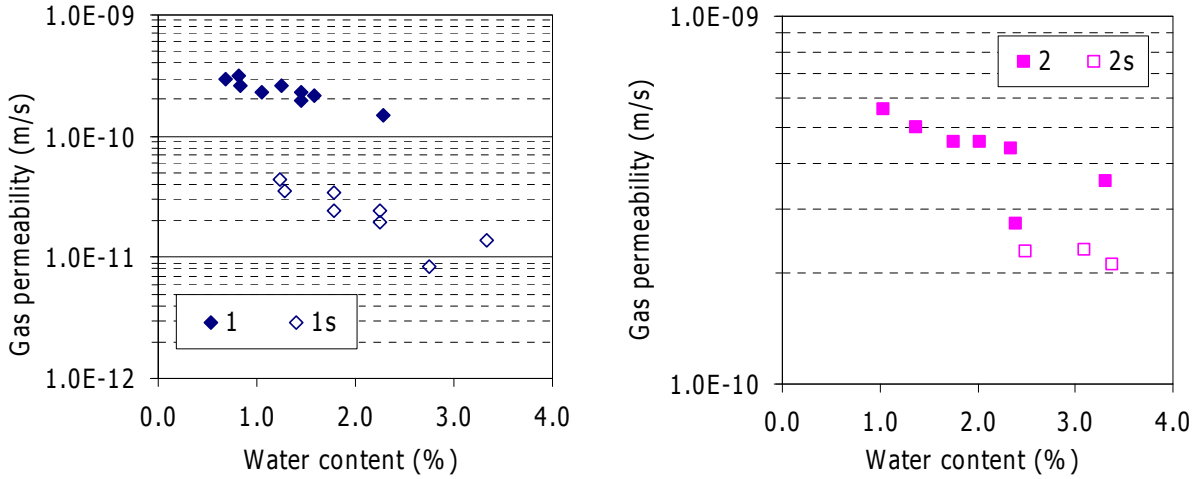

Figure 5: Evolution of gas permeability of samples 1 (left) and 2 (right) on drying before (1 and 2) and after water saturation (1s and 2s)

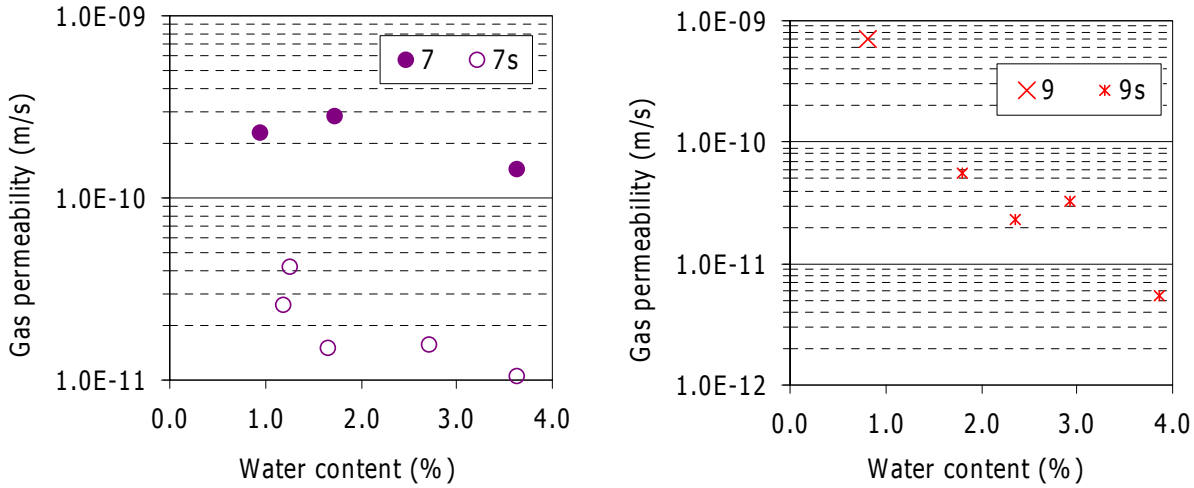

Figure 6: Evolution of gas permeability of samples 7 (left) and 9 (right) on drying, before (7 and 9) and after water saturation (7s and 9s)

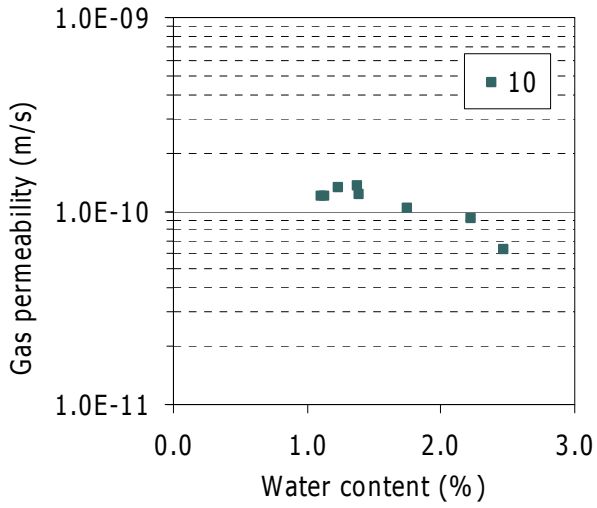

Figure 7: Evolution of gas permeability of sample 10 on drying

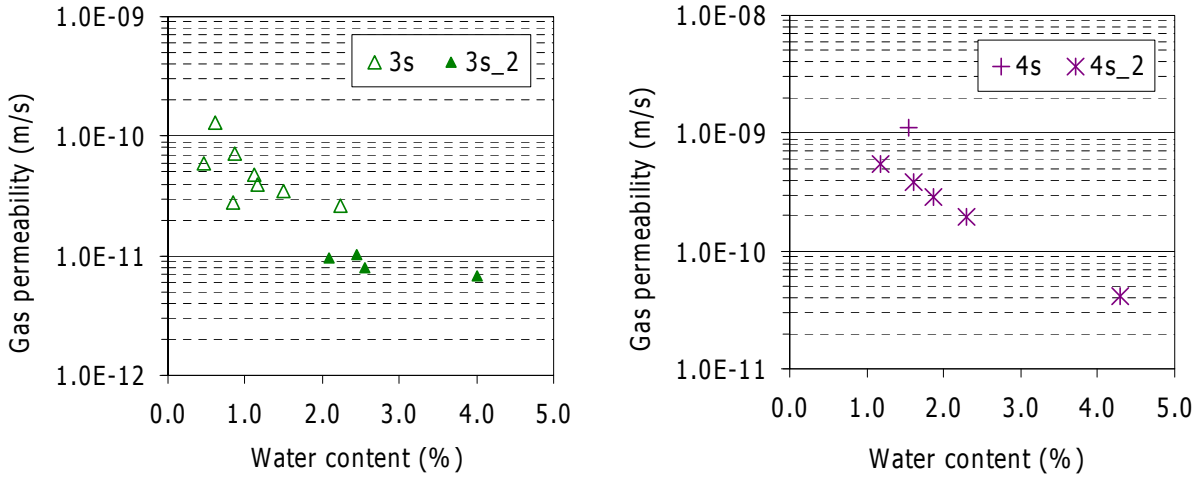

Figure 8: Evolution of gas permeability of samples 3 (left) and 4 (right) on drying, after water saturation (3s and 4s) and after drying and water resaturation (3s_2 and 4s_2)

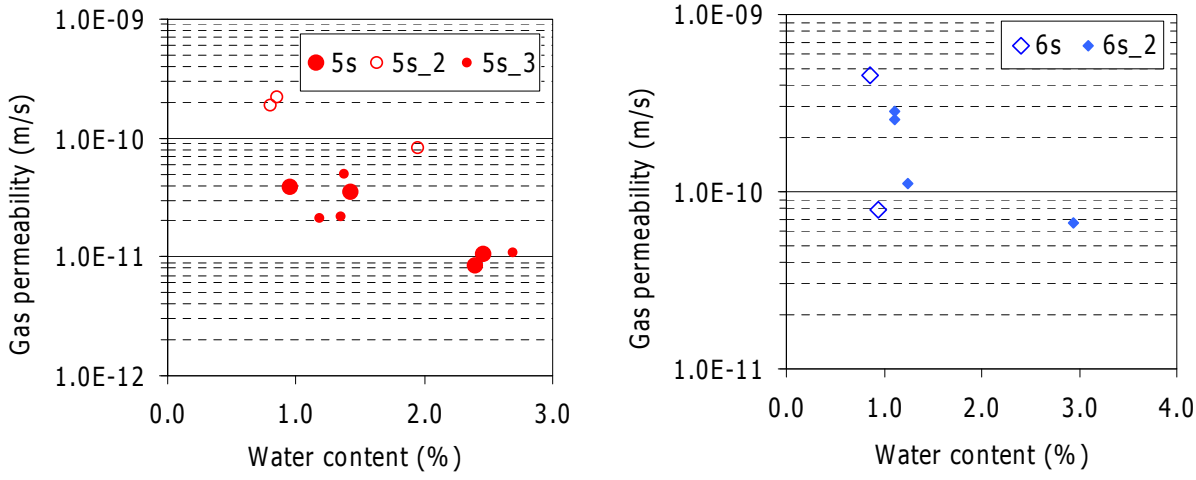

Figure 9: Evolution of gas permeability of samples 5 (left) and 6 (right) on drying, after water saturation (5s and 6s) and after drying and water resaturation (5s_2, 5s_3 and 6s_2)

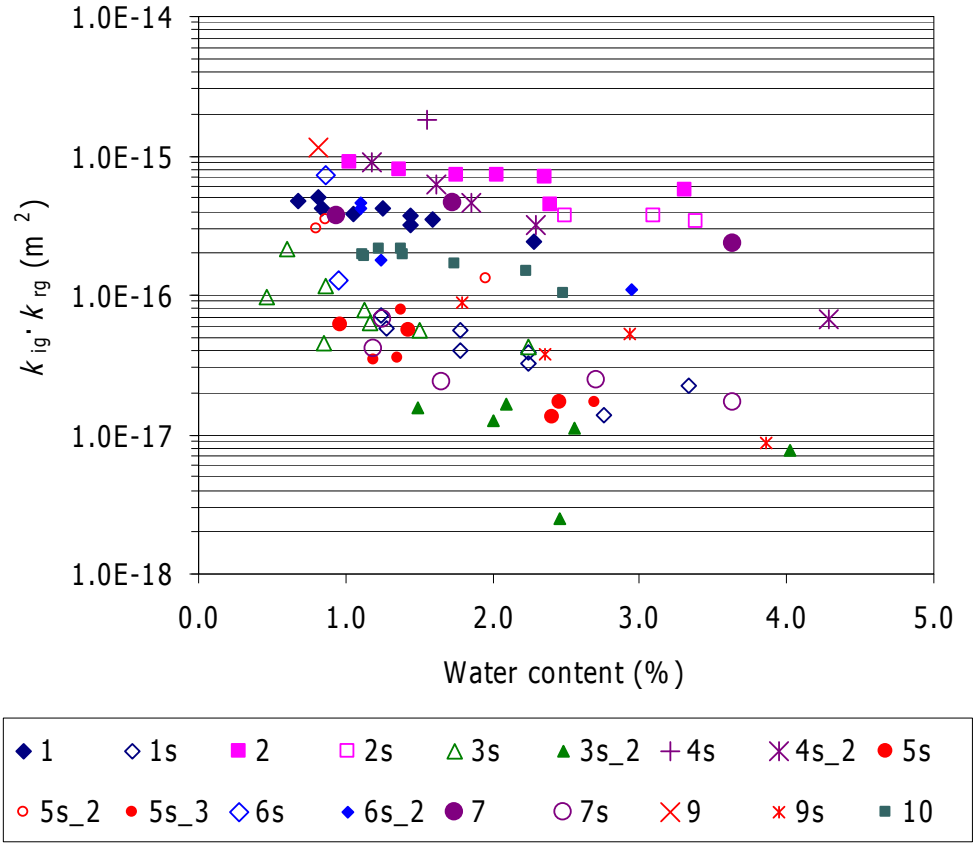

Figure 10: Concrete gas permeability ($k_{ig} \cdot k_{rg}$) as a function of water content during air drying (samples with an s in the reference were previously water saturated)

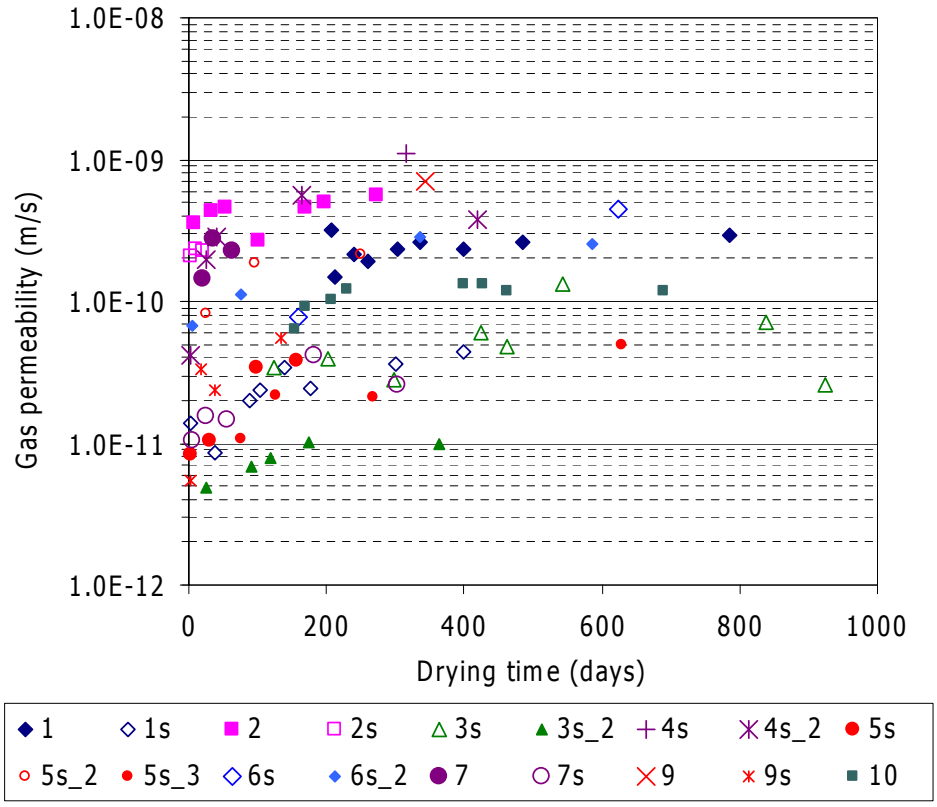

Figure 11: Concrete gas permeability (k_g) evolution during air drying (samples with an s in the reference were previously water saturated)

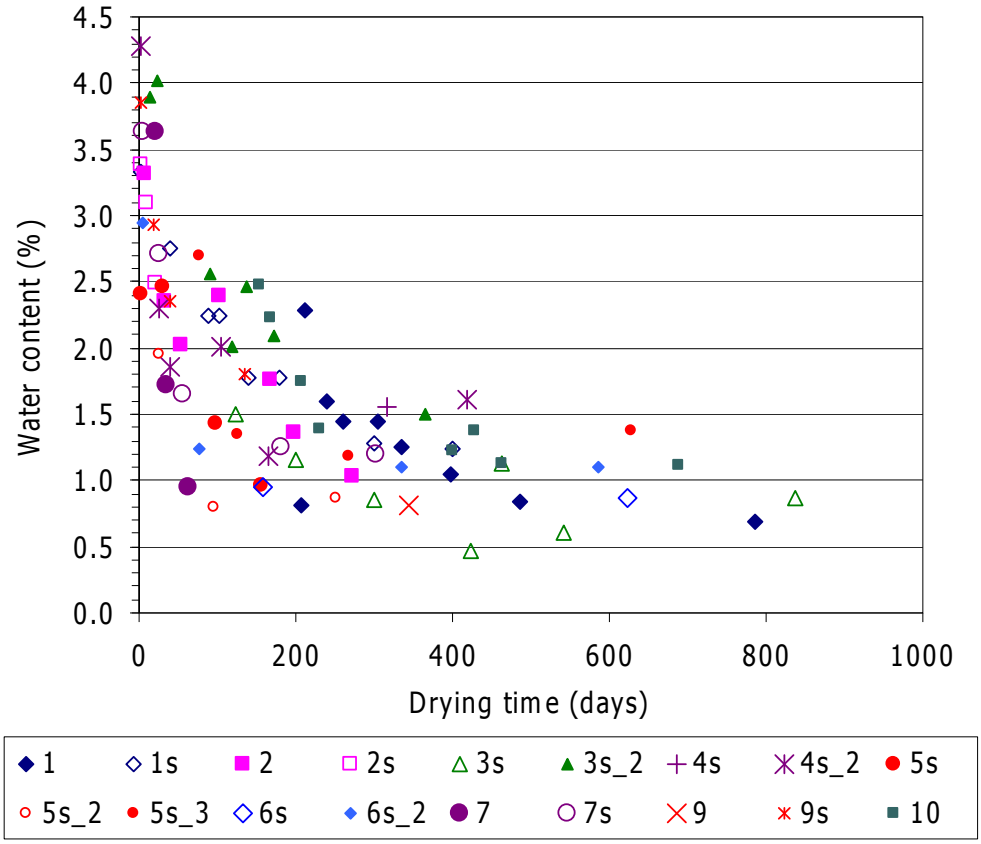

Figure 12: Evolution of water content during drying of the concrete samples (samples with an s in the reference were previously water saturated)

Overall, the permeability of samples that were not previously saturated was higher than that of those previously saturated. After saturation, the gas permeability tended to decrease, although this decrease was not so clear if the samples had been air-dried before saturation. This can be seen in Figure 13, where the results have been grouped according to the hydraulic history of the samples and fit to exponential curves. Also, the permeability increase on drying seems more acute in samples that were previously saturated. In this figure the values under the reference "saturated after air-drying" correspond to samples that had been saturated after air drying once, twice or thrice. These have been separated in Figure 14, where it can be observed that the number of wetting/drying cycles does not seem to affect the value of gas permeability.

The gas permeability is also usually related to the accessible void ratio of the material, which is computed as $e(1\text{-}S_r)$. These values are plotted in Figure 15, where it can be observed that the accessible void ratios of the samples tested are below 0.15, which is high if we take into account that the average void ratio of these concrete samples was 0.16 (see section Material). The relationship between permeability and accessible void ratio in samples not previously saturated is not clear, but for the other samples, there is a clear trend for the permeability to increase as the accessible void ratio does.

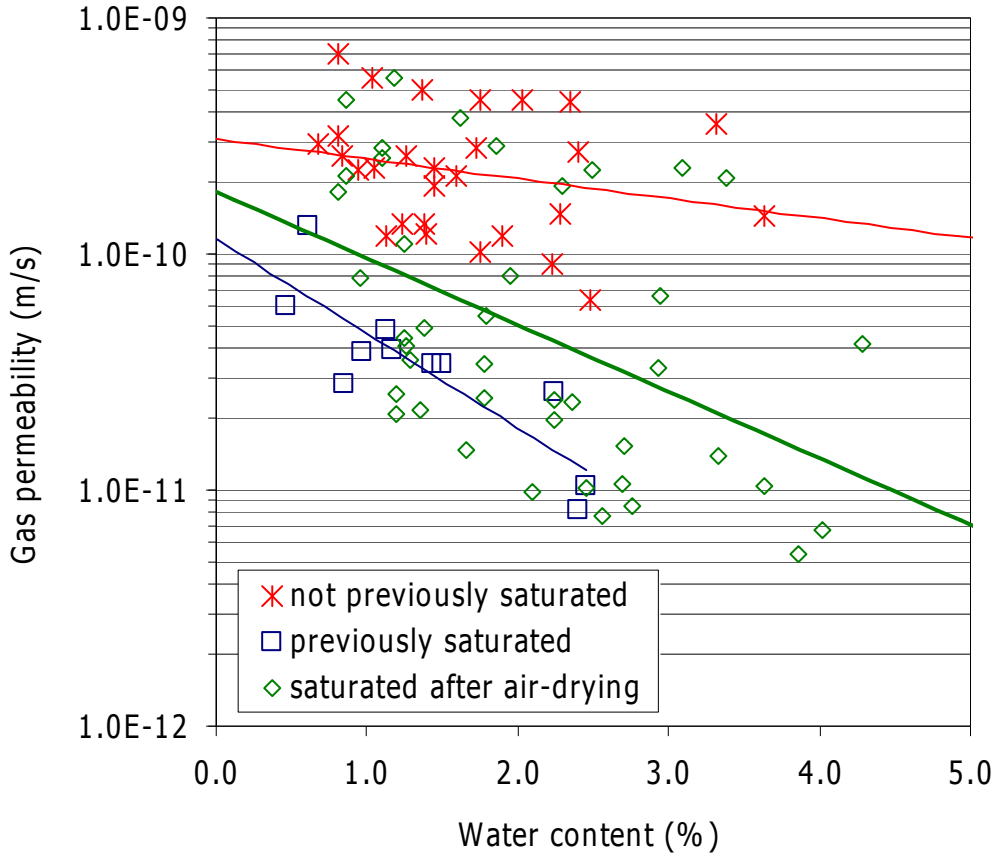

Figure 13: Change of gas permeability (k_g) with water content for samples with different hydraulic history

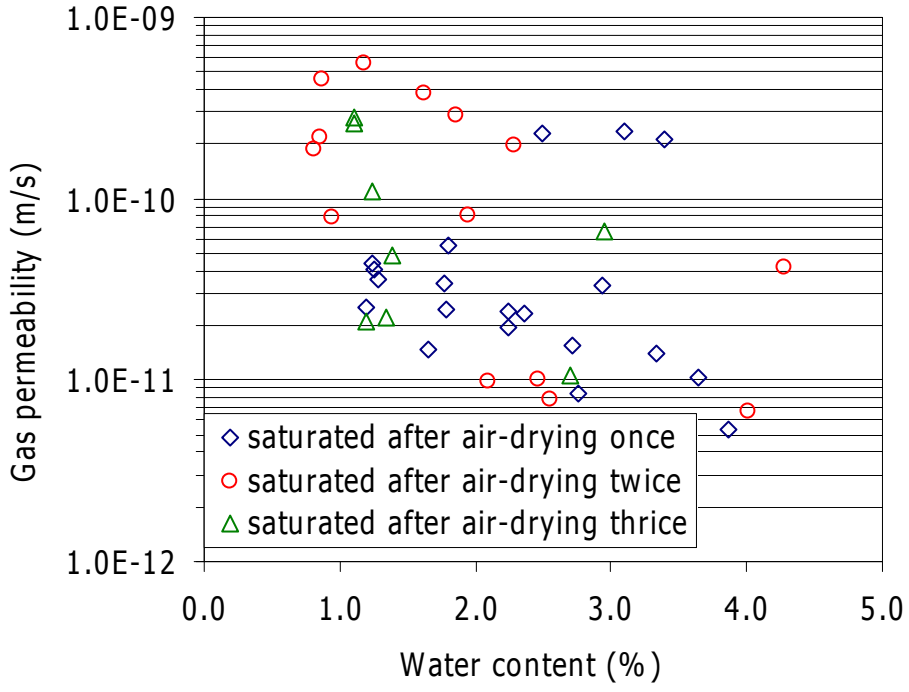

Figure 14: Change of gas permeability (k_g) with water content for samples saturated after air-drying

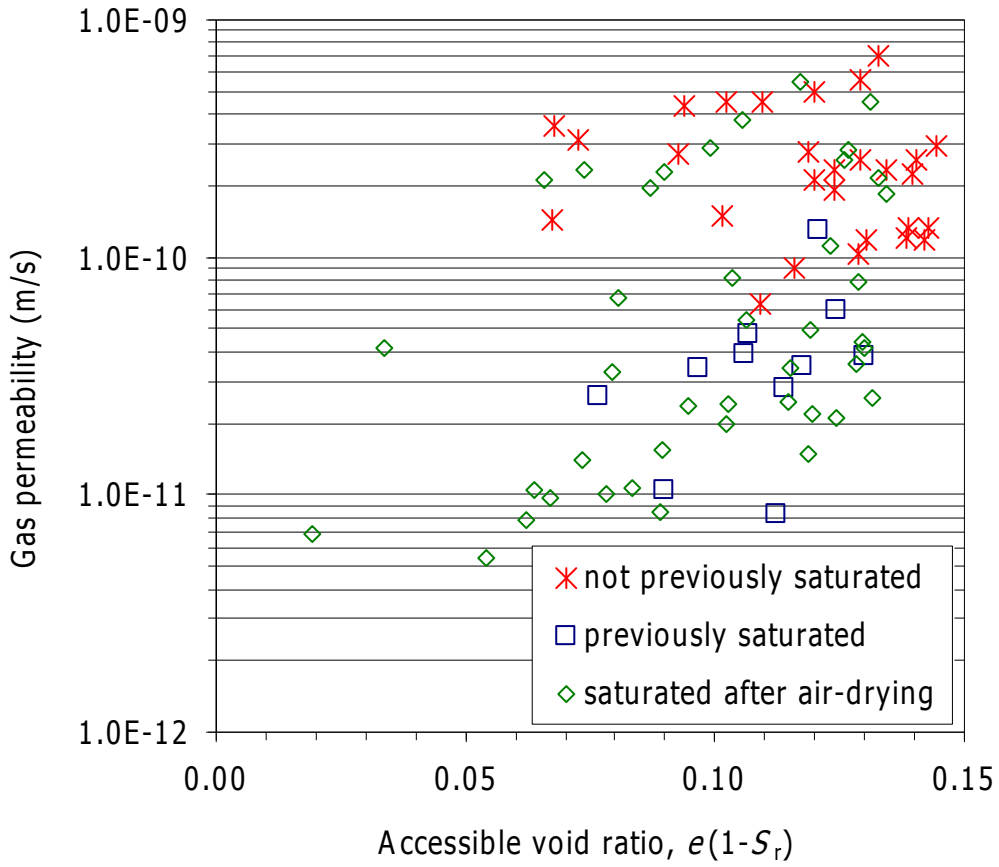

Figure 15: Change of gas permeability (k_g) with accessible void ratio for samples with different hydraulic history

4.1.2 Steady-state method

Some of the samples measured with the non-steady-state method were also measured in the steady-state equipment, in order to analyse the influence of boundary conditions such as injection, confining and backpressures, on the value of permeability. It was checked that for a given sample and test step the gas outflow was equal to the gas inflow, and thus the intrinsic permeability calculated was the same irrespective of the flow (in or out) used to compute it. However, when gas permeability was calculated taking into account the fluid properties (*i.e*. the permeability in m/s), the gas permeability upstream was usually slightly higher than downstream, up to a maximum of one order of magnitude when the upstream and downstream pressures were very different. This was due to the variation of the fluid properties with pressure and gave an idea of the possible range of variation of gas permeability inside the sample due to the gas pressure gradient.

Sample 3

Sample 3 was measured twice in the non steady-state equipment during the drying process. The sample water content in the first measurement (PG3_6, Table XIV) was 1.6 percent. Between this measurement and the next one in the steady-state equipment (PG3_7, Table XV), the sample was accidentally wetted, and this is why the water content in the latter measurement was higher (2.2 percent).

During the tests, the confining pressure was kept constant (at 400-500 kPa in the first test and 1500 kPa in the second one) and the backpressure was kept atmospheric (Figure 16). The

injection pressure was first gradually increased and then reduced. The results obtained in this phase for the two tests are shown in Figure 17. As expected, the sample with the higher water content showed the lower gas permeability. The values obtained during the pressure increase were equal to those found on pressure reduction. Permeability decreased slightly at the beginning of the injection pressure increase cycle. Also, the $k_{ig} \cdot k_{rg}$ values calculated with the inflow or the outflow for a given pressure condition were equal, whereas the k_g calculated with the inflow was not the same as that calculated with the outflow, since the gas density in both cases is different due to the pressure difference between top and bottom of the sample. Figure 17 shows also the permeability determined in the unsteady-state equipment in the sample with the same water content. In both cases that value is higher, what could be due to the very low injection pressure in the tests performed in the unsteady-state equipment.

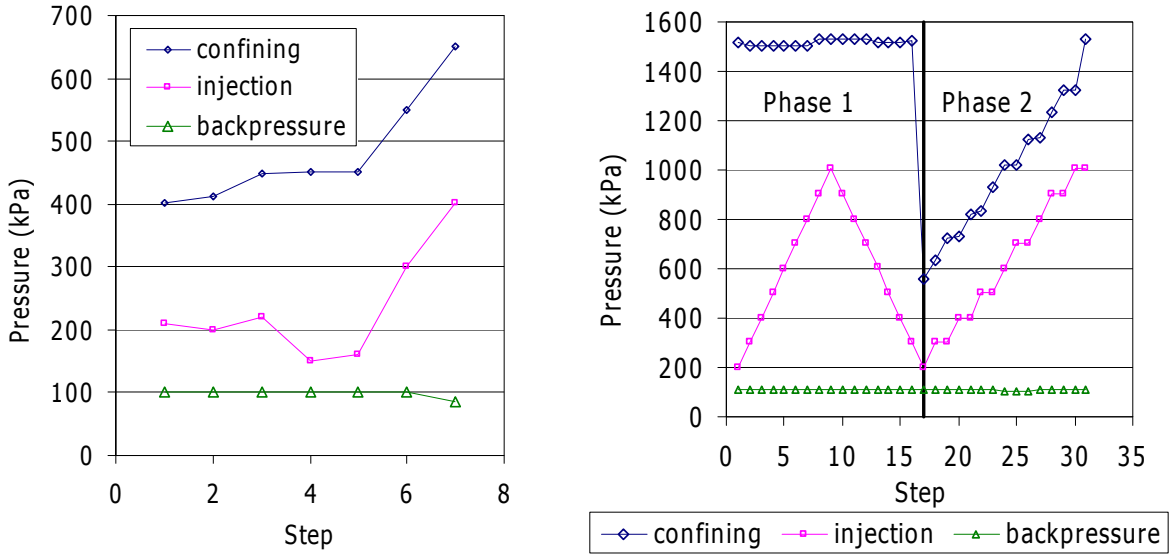

Figure 16: Stress paths followed in the tests with sample 3 in the steady-state equipment (left: test PG3_6, right: test PG3_7)

In test PG3_7, after the pressure cycle under constant confining pressure, the confining pressure and the injection pressure were reduced to 500 and 200 kPa, respectively, and then increased gradually and simultaneously to 1500 and 1000 kPa, respectively (Figure 16, right, phase 2). In this way, two different effective stresses were applied. For a given effective stress, the gas permeability decreased slightly as the injection and confining pressures increased (Figure 18).

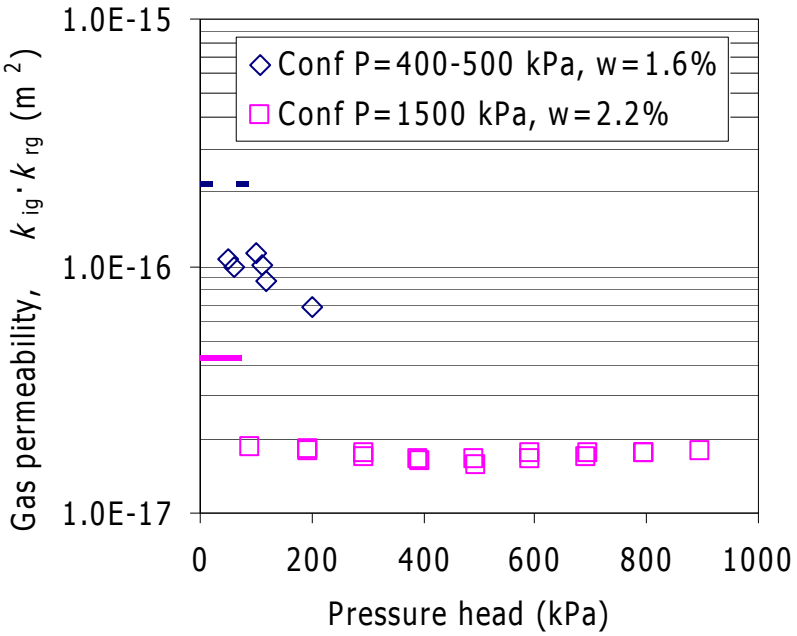

Figure 17: Change of gas permeability ($k_{ig} \cdot k_{rg}$) with injection pressure for sample 3 at different water contents and constant confining pressures. Atmospheric backpressure. The values obtained with the unsteady-state equipment are shown with dotted horizontal lines

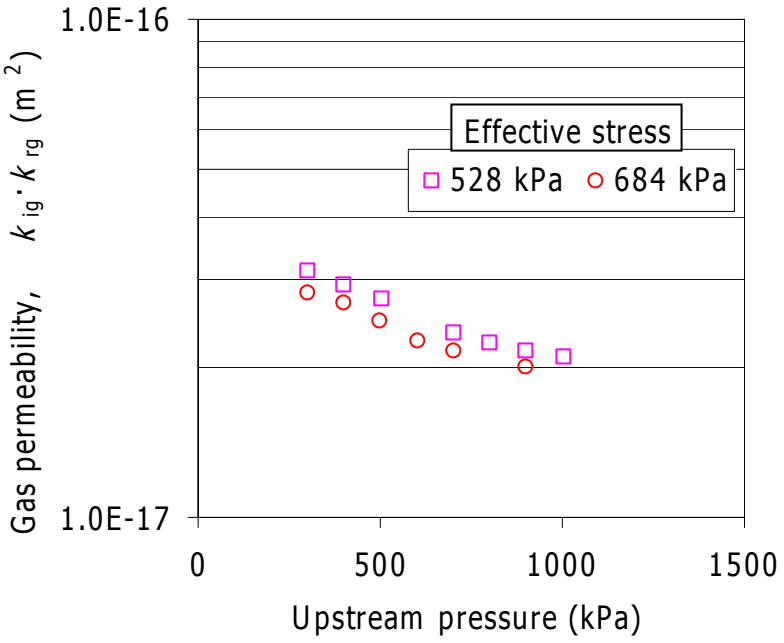

Figure 18: Evolution of gas permeability ($k_{ig} \cdot k_{rg}$) for sample 3 (test PG3_7) as confining and injection pressure increased while backpressure remained atmospheric

Sample 5

Sample 5 was initially saturated to determine hydraulic conductivity and then it was air dried, measuring gas permeability as the water content decreased with the unsteady-state equipment (Table IX, Appendix 1). Then the sample was saturated again to measure for a second time the water permeability and it was afterwards again air dried. Twice during this second air drying

process the sample was tested in the steady-state equipment, with two different water contents, 1.9 and 0.9 percent.

A summary of the values obtained during the first measurement is shown in Table XVI (PG5_6). In test PG5_6 the backpressure was initially kept constant at 174 kPa while the injection pressure was increased under a constant confining pressure of 700 kPa (Phase 1); afterwards, the backpressure was increased and then decreased while injection pressure was kept constant at 800 kPa and the confining pressure at 1000 kPa (Phase 2); and finally, keeping a constant backpressure of 200 kPa and a confining pressure of 1000 kPa, the injection pressure was reduced (Phase 3) (Figure 19, left). After each pressure change flow became quickly stable and for this reason the duration of each step was usually of just a few hours.

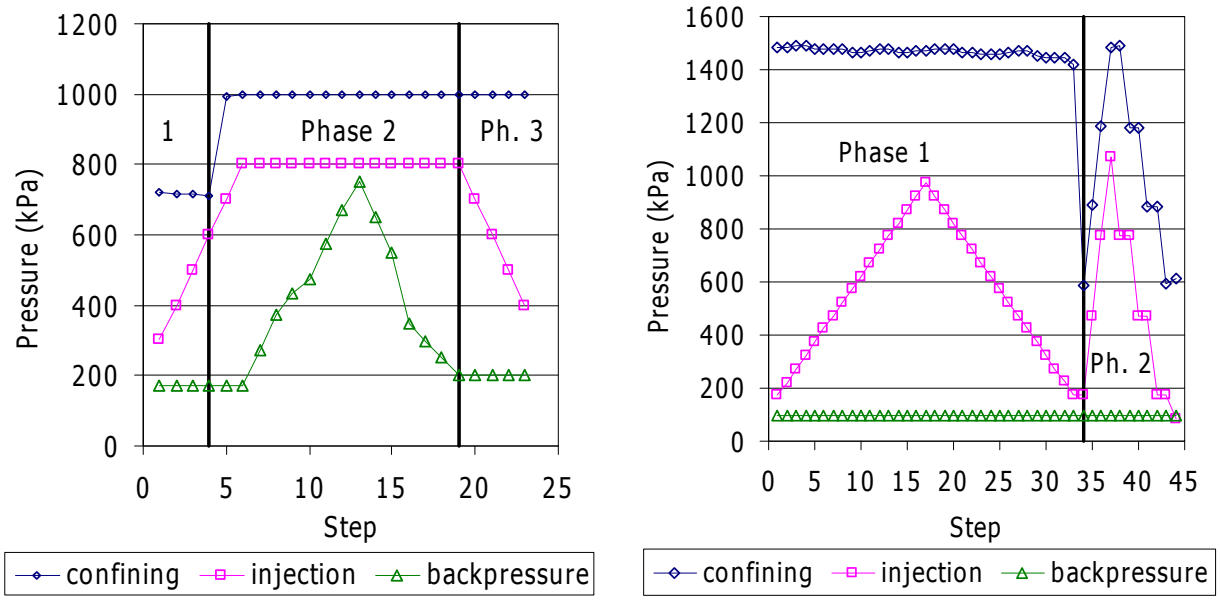

Figure 19: Stress paths followed in the tests with sample 5 in the steady-state equipment (left: test PG5_6, right: test PG5_8)

The permeability values obtained during the test calculated from the gas outflow, both in terms of k_g and $k_{ig} \cdot k_{rg}$, are plotted in Figure 20 as a function of the pressure head. All the values were lower than those determined with the unsteady-state method for the same water content. The intrinsic permeability tended to be lower in Phase 2 and 3, when the confining pressure was higher, than in Phase 1. When the injection pressure was kept constant at 800 kPa (Phase 2), k_g decreased as the pressure head increased (*i.e*. as backpressure decreased), but it remained approximately constant when the fluid properties were not taken into account ($k_{ig} \cdot k_{rg}$). When the backpressure was kept constant and the injection pressure varied, permeability did not show a clear dependence on pressure head. For low pressure heads, there was a significant difference between the gas permeability values obtained for low and high backpressures, those obtained for high backpressures being higher. Thus, the determining factor for the permeability increase seemed to be the backpressure, which was the one predominant inside the sample.

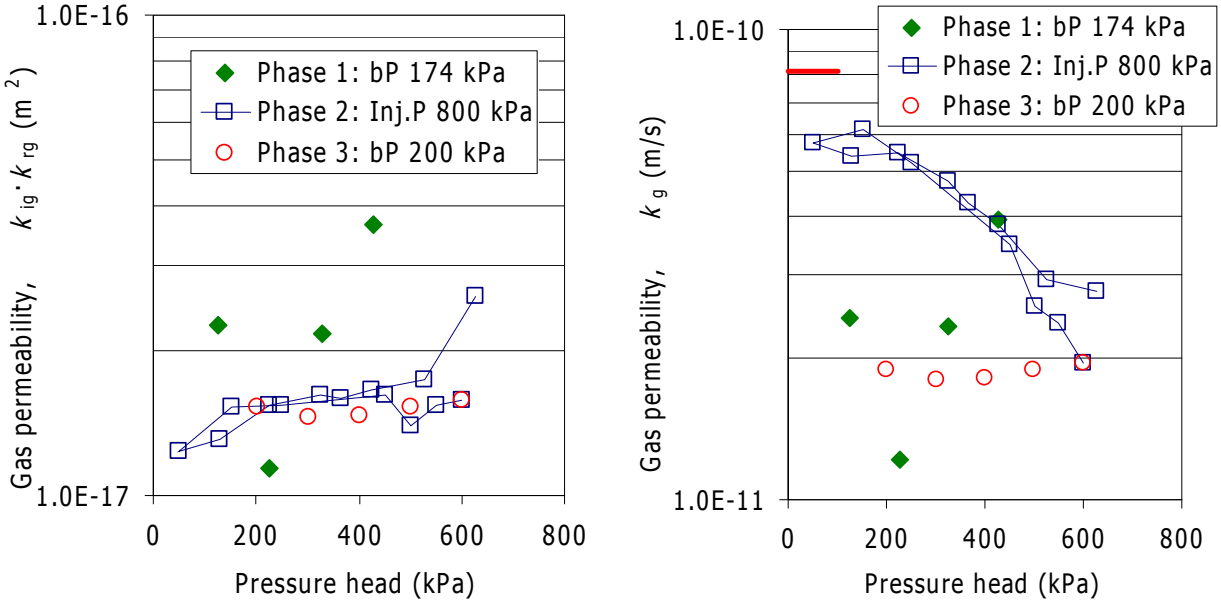

Figure 20: Gas permeability calculated from outflow during test PG5_6 (ρ_d=2.32 g/cm^3, *w*=1.9%). Confining pressure was 700 kPa in Phase 1 and 1000 kPa in Phase 2 and 3. The thick horizontal line is the value determined in the unsteady-state equipment. bP: backpressure, Inj.P: injection pressure

The results obtained during the second measurement, performed with a water content of 0.9 percent, are shown in Table XVII (PG5_8). There were two phases in this test: in Phase 1, under a constant confining pressure of 1500 kPa and atmospheric backpressure, the injection pressure was gradually increased and then decreased; during Phase 2, both confining pressure and injection pressure were increased and later decreased simultaneously (Figure 19, right).

The values obtained during Phase 1 as computed from the gas inflow and outflow are plotted in Figure 21, both in terms of $k_{ig} \cdot k_{rg}$ and k_g, along with the value obtained in the unsteady-state method. The difference between the values obtained in terms of k_g from the inflow and the outflow, which was significant, came from the change of gas density with pressure. This difference was not observed for the intrinsic permeability values, except for pressure heads below 300 kPa. Since backpressure was kept atmospheric, the k_g values calculated from the outflow were not affected by the gas density change, although they showed a dependence on injection pressure for the low pressure heads (permeability decreased with injection pressure increase up to a pressure head of 400 kPa). The values obtained during the injection pressure increase and decrease were the same for the same pressure head values.

Besides, the values were slightly higher than those determined in test PG5_6, due to the higher water content in the latter (Figure 22). The difference was not very important though, maybe because the confining pressure applied was higher in test PG5_8 and gas permeability is very sensitive to it.

During Phase 2 of test PG5_8, permeability decreased as the confining pressure and injection pressures increased, and the values obtained were lower when the pressure inside the sample, taken as the difference between the confining and the injection pressures, was higher (Figure 23). All the values were lower than the value obtained in the unsteady-state equipment for the same water content.

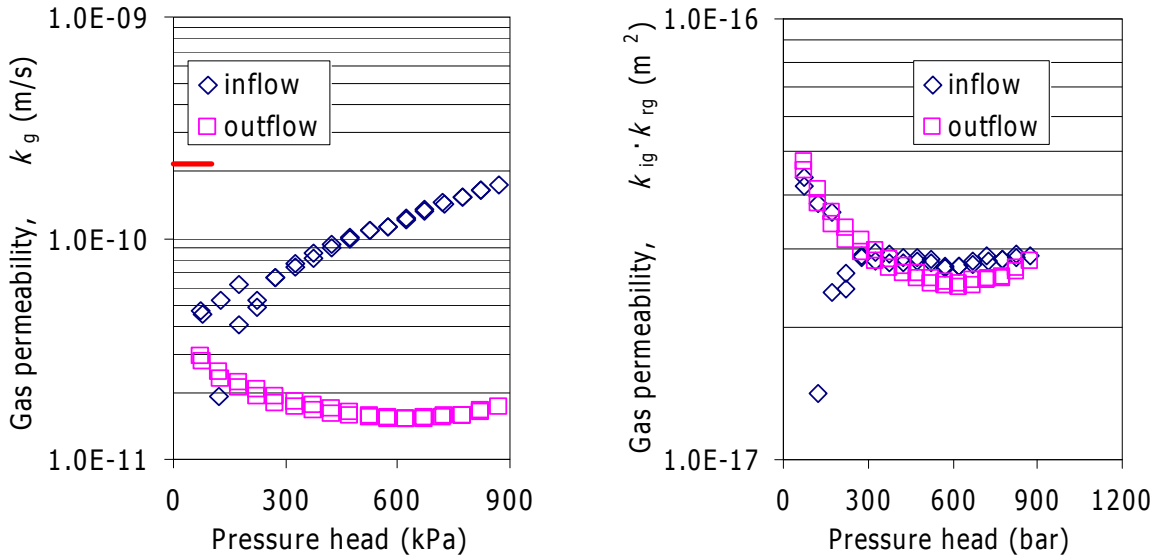

Figure 21: Gas permeability calculated from inflow and outflow during Phase 1 of test PG5_8 (ρ_d=2.32 g/cm^3, *w*=0.9%). Confining pressure was 1500 kPa and backpressure atmospheric, injection pressure was increased and decreased. The thick horizontal line is the value determined in the unsteady-state equipment

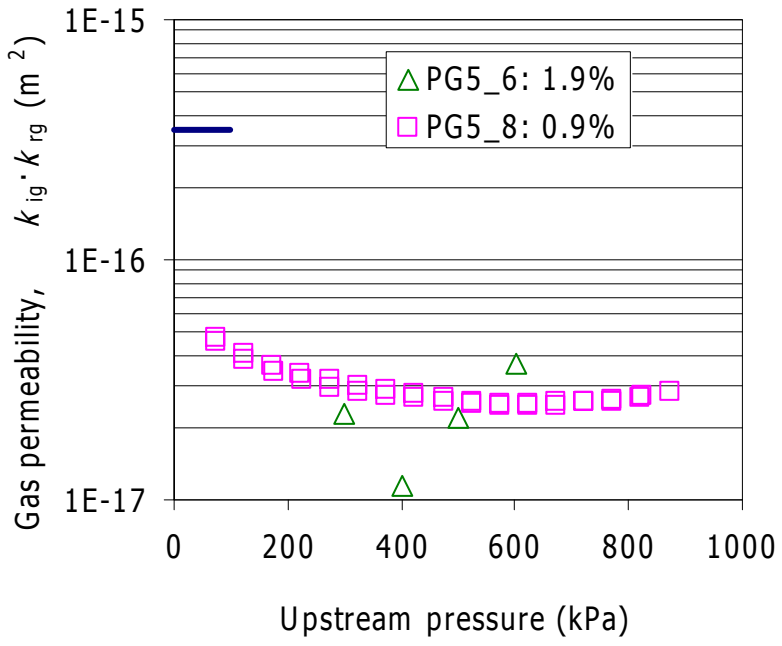

Figure 22: Gas intrinsic permeability obtained for sample 5 (ρ_d=2.32 g/cm^3) with water content 1.9% under a confining P of 800 kPa and backP 170 kPa (test PG5_6, Phase 1) and with water content 0.9% under a confining P of 1500 kPa and backP 100 kPa (test PG5_8, Phase 1). The thick horizontal line is the value determined in the unsteady-state equipment

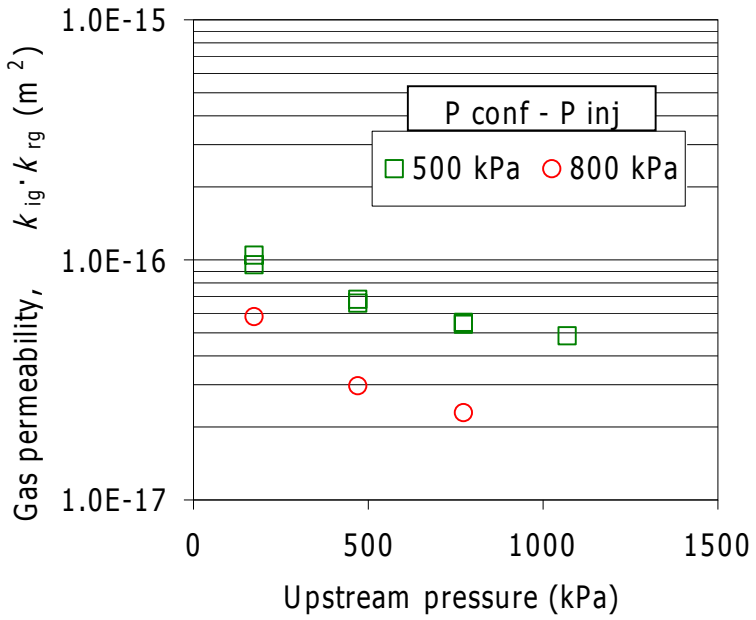

Figure 23: Gas intrinsic permeability obtained for sample 5 (ρ_d=2.32 g/cm^3) with water content 0.9% under changing injection and confining pressures and atmospheric backpressure (test PG5_8, Phase 2)

Sample 7

Sample 7 was measured with a water content of 1.2 percent in two phases, in both of them the backpressure was kept atmospheric. In Phase 1 the injection and the confining pressures were simultaneously increased, so that to keep a constant difference between confining and injection pressures of 300 kPa. In Phase 2 the confining pressure was kept constant (1400-1600 kPa) and the injection pressure was gradually decreased (Figure 24). The results obtained in both phases are summarised in Table XVIII (Appendix 1) and plotted in Figure 25.

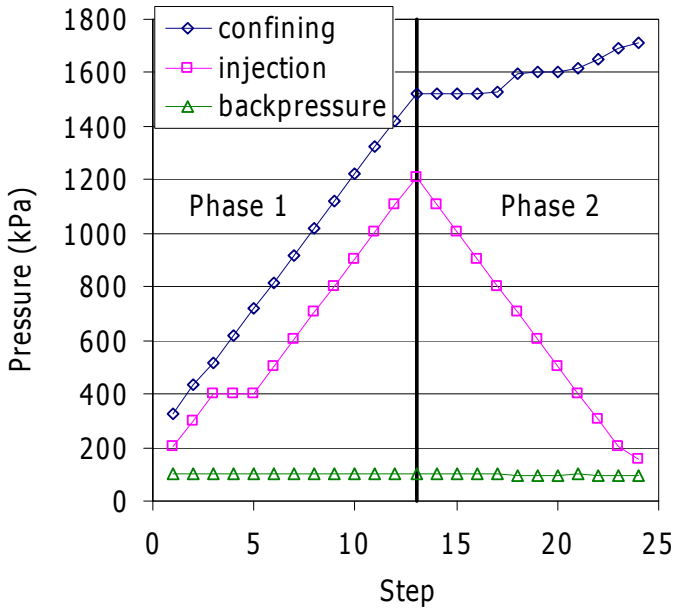

Figure 24: Stress path followed in test PG7_3 with sample 7 in the steady-state equipment

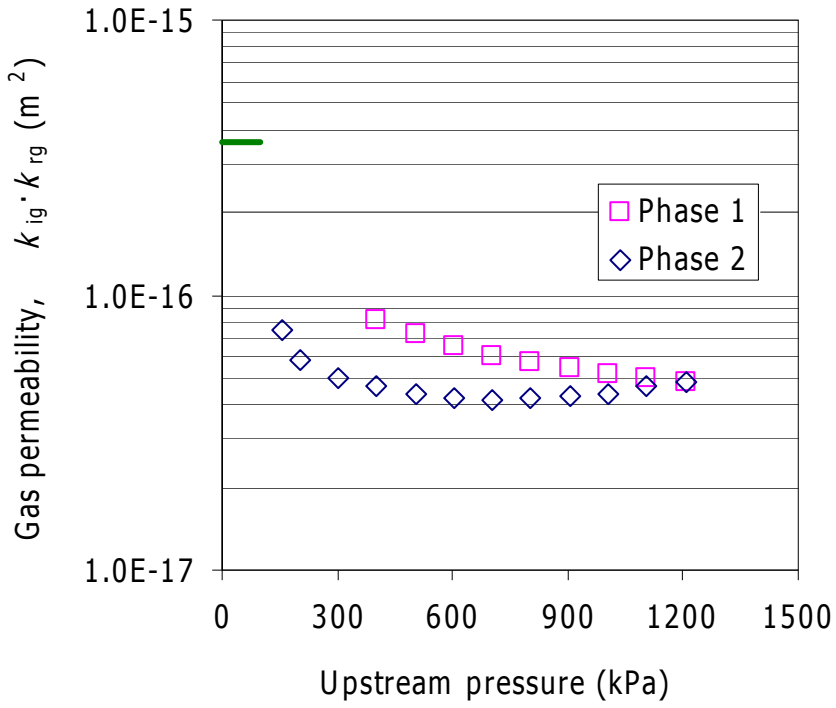

Figure 25: Gas intrinsic permeability during test PG7_3 (ρ_d=2.30 g/cm^3, *w*=1.2%). Atmospheric backpressure. Phase 1: confining and injection pressures increased simultaneously, Phase 2: confining pressure at 1400-1600 kPa, injection pressure decreased. The thick horizontal line is the value determined in the unsteady-state equipment

In the first phase, under constant confining stress, gas permeability increased with injection pressure decrease. In the second phase, gas permeability increased with injection pressure decrease and effective stress increase, especially for the low injection pressures.

Samples 9 and 10

Samples 9 and 10 were tested immediately after they were taken out of the wet chamber, however they showed high permeability, both when tested with the unsteady-state method (Table XII and Table XIII, Appendix 1) and with the steady-state one, probably because the relative humidity in the chamber was not very high and consequently, the water content of the concrete was not as high as expected. The results obtained in the steady-state equipment are summarised in Table XIX and Table XX (Appendix 1). Both samples were tested initially under a confining pressure of 1500 kPa and atmospheric backpressure while the injection pressure was gradually increased (Figure 26). The results obtained during this phase in both samples are plotted in Figure 27. The gas permeability kept constant for sample 9 despite the injection pressure change, while it decreased for sample 10 as injection pressure increased. Sample 10 was not further tested, since the gas flow was so high that the pressure steps could not be kept for long. Sample 9 was subjected to a second testing phase in which the confining and the injection pressures were decreased in subsequent steps, in a proportion that made the hydraulic head and the average stress inside the sample also to decrease (Figure 28). As observed in other tests, the gas permeability increased as confining and injection pressure decreased.

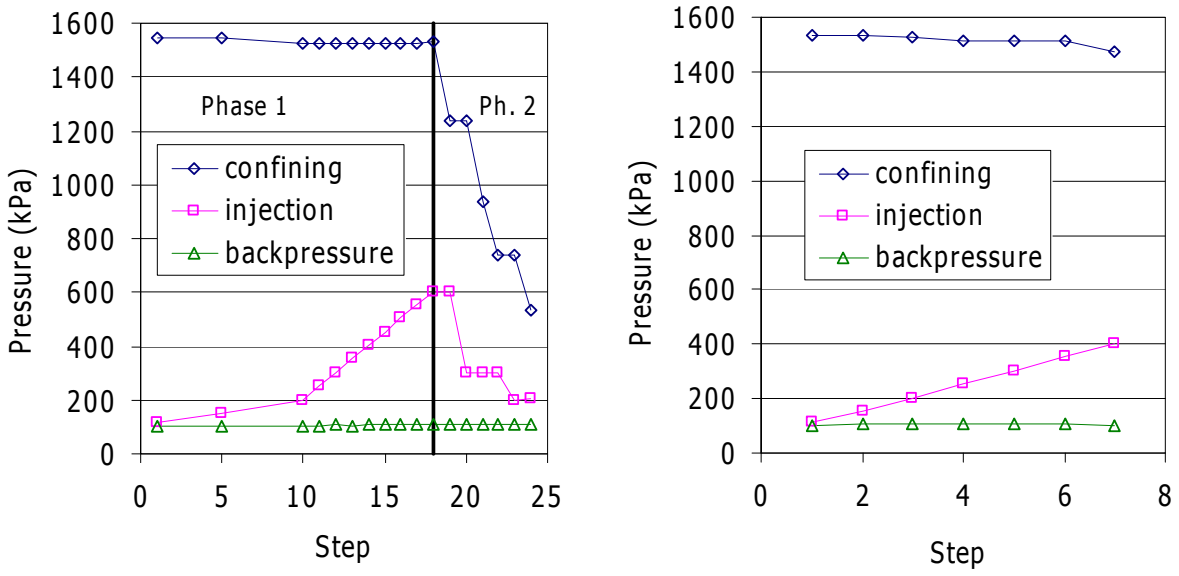

Figure 26: Stress paths followed in the tests with samples 9 (left: test PG9_2) and 10 (right: test PG10_1) in the steady-state equipment

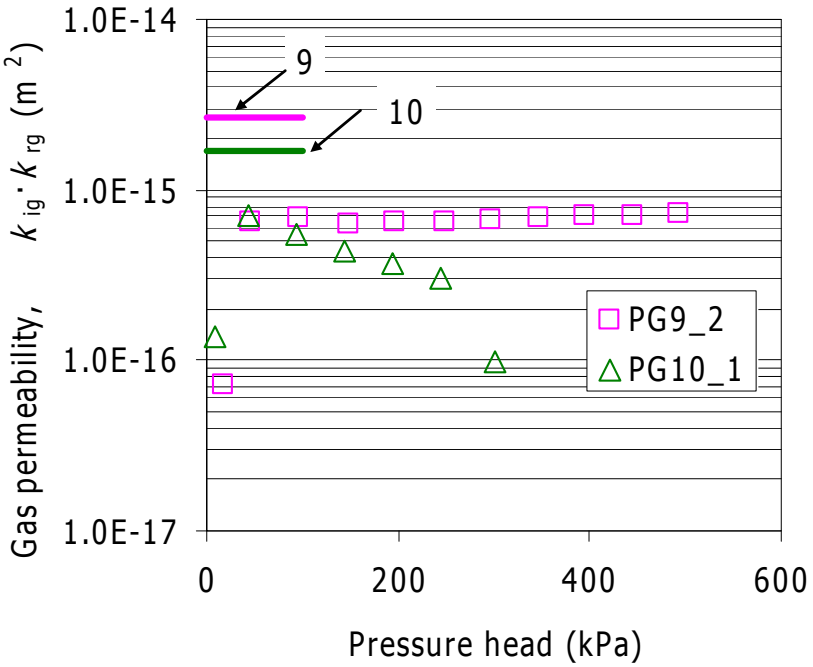

Figure 27: Gas intrinsic permeability calculated for samples 9 (ρ_d=2.32 g/cm^3, *w*=1.1%) and 10 (ρ_d=2.28 g/cm^3, *w*=4.0%). Atmospheric backpressure, confining pressure 1500 kPa. The thick horizontal lines are the values determined in the unsteady-state equipment

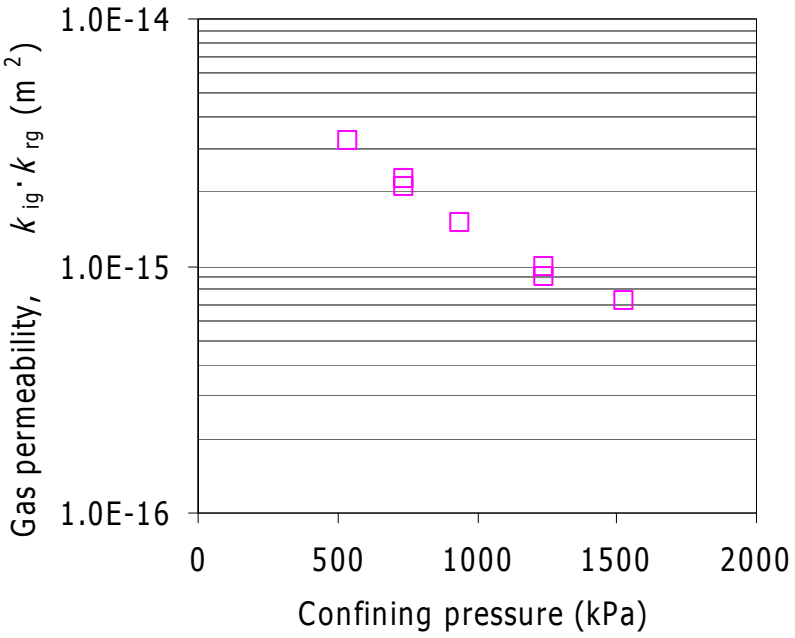

Figure 28: Gas intrinsic permeability for sample 9 in Phase 2 of test PG9_2 (ρ_d=2.32 g/cm^3, *w*=1.1%). Atmospheric backpressure, confining and injection pressures decreased simultaneously

4.2 WATER PERMEABILITY

The hydraulic conductivity of these samples was measured after saturating them with deionised water. The tests were performed at room temperature (22±2 °C) in a constant head permeameter, applying hydraulic gradients of 185±34. The details of each measurement are given in Appendix 1 (Table XXI), where the initial and final water contents and degree of saturations are given, along with the water permeability (k_w), the intrinsic permeability obtained from liquid flow (k_{iw}) and the time needed to reach a stable permeability value. It was observed that normally, the longer the saturation time the lower the hydraulic conductivity (Figure 29). In some instances it took about 100 days to get a stable permeability value. Some of the samples were saturated immediately after taking them from the wet room (samples 0, 3, 4 and 5), and others after air drying and gas permeability measurement. This process was repeated twice for samples 3 and 4, and thrice for sample 6. The second time the hydraulic conductivity was determined, *i.e*. after previous saturation and air drying, the value obtained was much lower (up to two orders of magnitude), although the difference between both values tended to be lower over time.

From these measurements, which were performed in saturated samples, the intrinsic permeability can be directly derived from Equation 6. The values obtained for the measurements corresponding to the longer saturation times are shown in Figure 30. The hydraulic history of the samples did not seem to affect the intrinsic permeability obtained from water flow. The two highest values corresponded to samples saturated during short time periods. Excluding these two values the range of intrinsic permeability values would be between $2 \cdot 10^{-17}$ and $5 \cdot 10^{-19}$ m^2, with an average value of $3.6 \cdot 10^{-18}$ m^2.

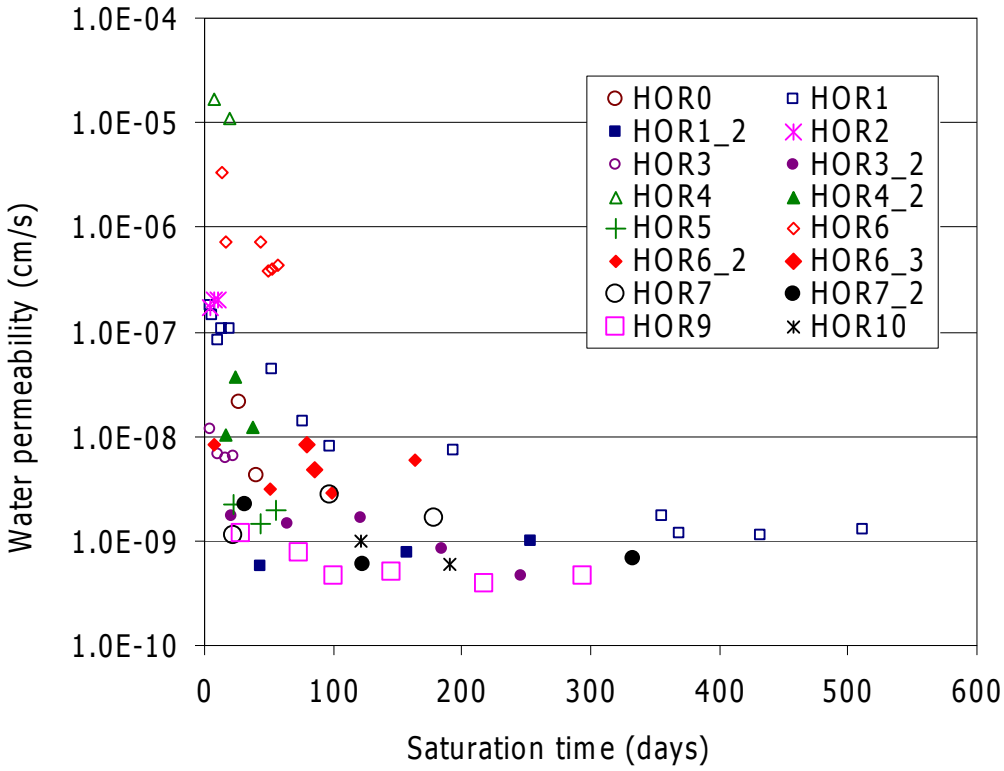

Figure 29: Hydraulic conductivity of the concrete samples measured after different times of saturation. All the measurements performed on previously air-dried samples, except HOR0, HOR3, HOR4 and HOR5 (for detailed hydraulic history refer to Table II)

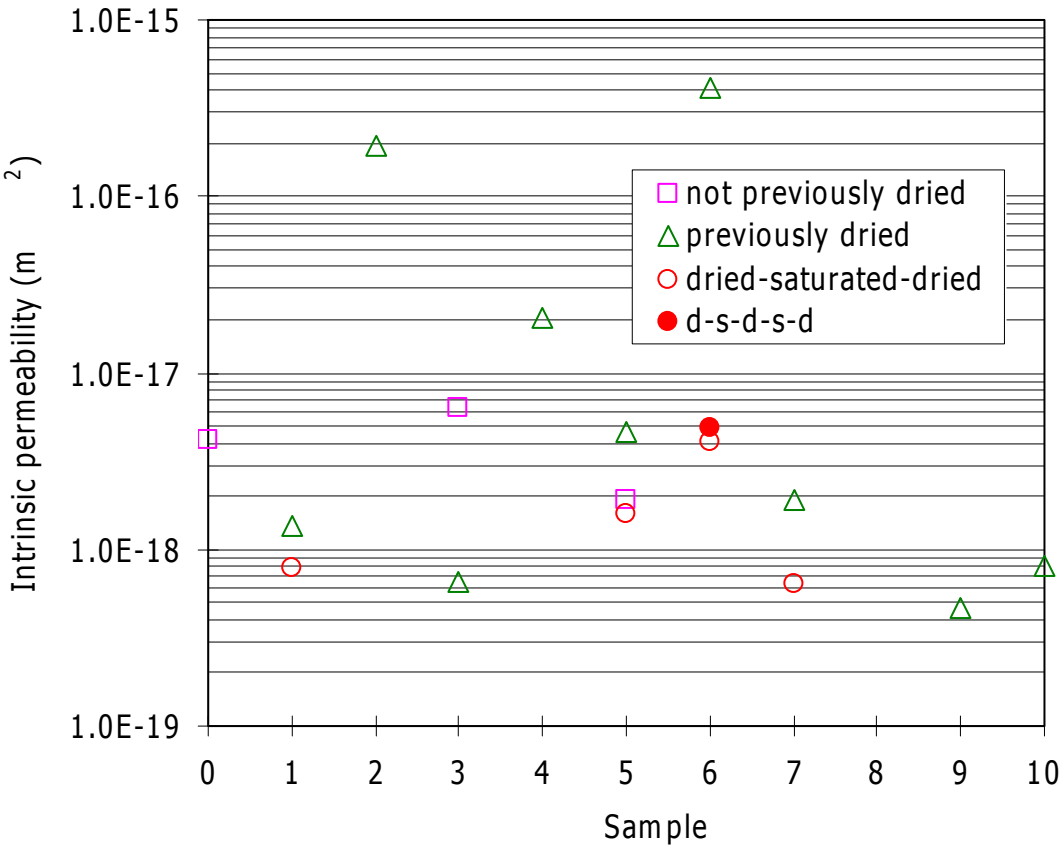

Figure 30: Intrinsic permeability obtained from water flow in the concrete samples

5 Discussion

5.1 ANALYSIS OF THE KLINKENBERG EFFECT

In gas flow through permeable materials with small pores, the mean free path of the molecules (that is, the mean distance between kinetic collisions) may become comparable to the pore size. The viscous drag is no longer transferred completely to the pore walls and the flow behaves as though there were slippage at the gas-solid interface. It is acknowledged that this would lead to the measured permeability becoming a function of pressure and to an overestimation in the permeability known as the gas slippage or the Klinkenberg effect. It is corrected for by making permeability measurements with gas at multiple pressure differences and constructing a graph of the measured apparent permeability (k_{ig}·k_{rg}) against the reciprocal of the mean pressure in the samples. The mean pressure (P_{mn}) is the average of the upstream (P_{up}) and downstream (P_{dw}) pressures in Equation 3. The points should lie on a straight line which intersects the *y*-axis at $1/P_{mn} = 0$. This value effectively represents the permeability at which the gas is compressed by infinite pressure and becomes a near perfect liquid and is known as Klinkenberg apparent permeability.

This method was applied for the tests performed with the steady-state equipment, in which different upstream and downstream pressures were applied to measure gas permeability. The results were grouped according to the effective confining pressure applied and are shown in Figure 31 for tests PG3_6 and PG3_7 (Table XIV and Table XV), in Figure 32 for tests PG5_6 and PG5_8 (Table XVI and Table XVII), in Figure 33 for test PG7_3 (Table XVIII) and in Figure 34 for tests PG9_2 and PG10_1 (Table XIX and Table XX). These Figures show in addition the effect of effective pressure on permeability, which clearly decreased when it reached values around 1000 kPa. The apparent permeability values obtained applying the Klinkenberg method are shown in Table III and plotted in Figure 35, along with the average of all the permeability values measured for a given effective confining pressure and the value obtained for the same samples with the unsteady-state equipment. The Klinkenberg apparent permeability obtained for a given effective pressure was only slightly smaller (by an average factor of 1.5) than the average of all the values measured for the same effective pressure range. This would mean that the injection and backpressures applied did not have a large influence on permeability. For this reason it is considered that the Klinkenberg effect was not relevant in the range of pressures applied.

Nevertheless, the values obtained with the steady-state method are lower than those obtained for the same samples with the same water content with the unsteady-state method, in which lower pressures were applied and the effective pressures were between 500 and 600 kPa. Despite the fact that higher permeabilities are expected for lower effective pressures, this difference between the two methods could also be partially explained if the Klinkenberg effect were relevant, since the possible overestimation of permeability arisen for not taking into account this effect takes place at low pressures.

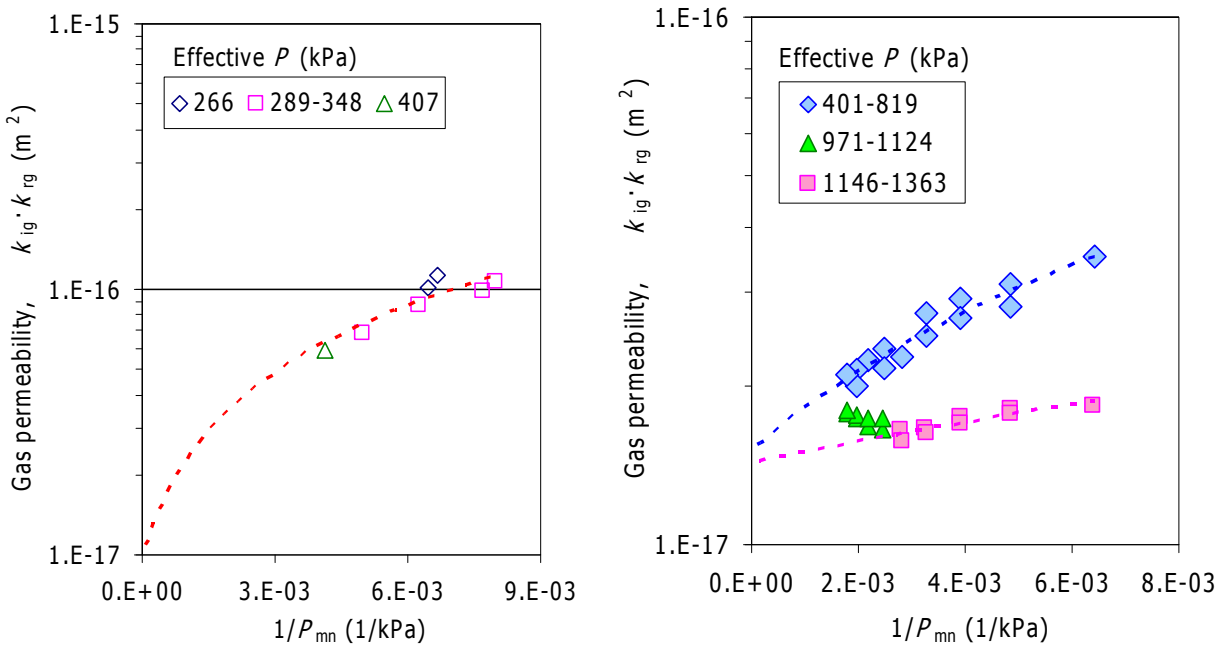

Figure 31: Measured permeability versus inverse of mean pressure (P_{mn}) for tests PG3_6 (left) and PG3_7 (right)

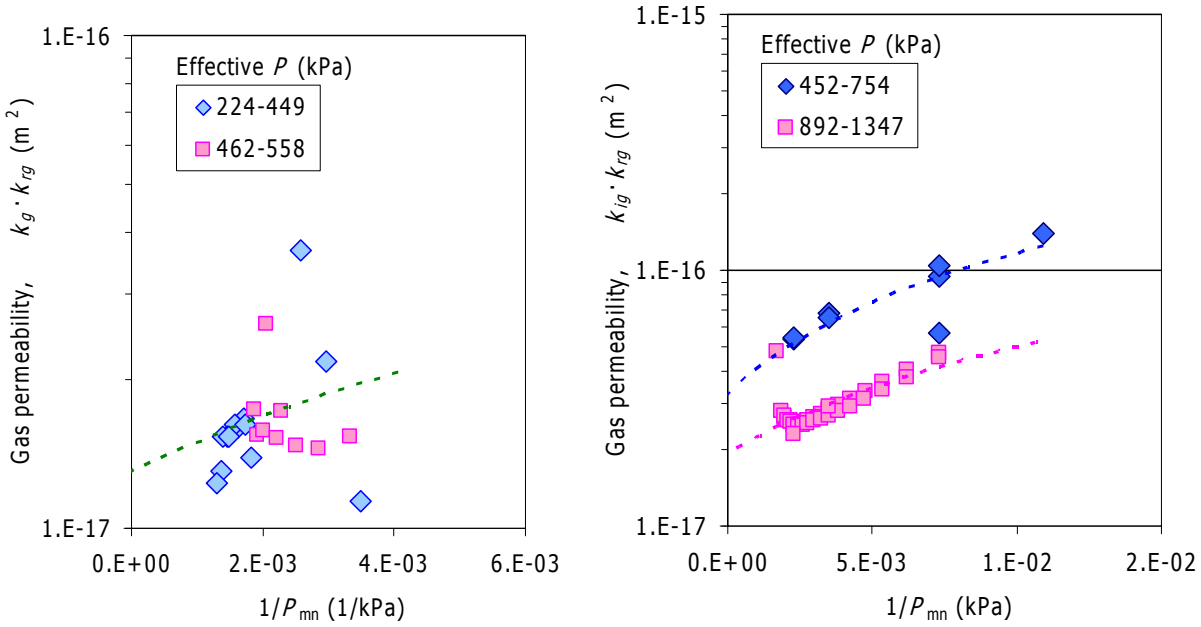

Figure 32: Measured permeability versus inverse of mean pressure (P_{mn}) for tests PG5_6 (left) and PG5_8 (right)

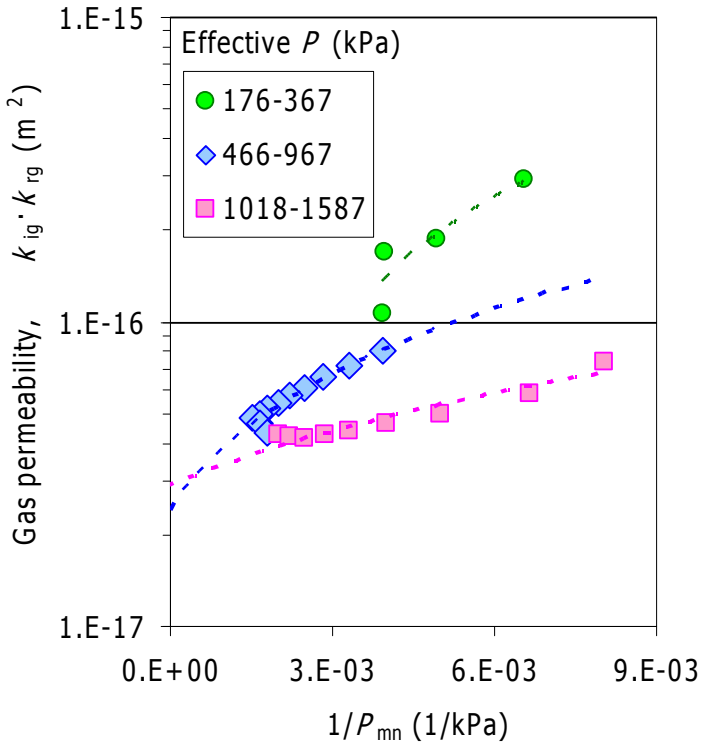

Figure 33: Measured permeability versus inverse of mean pressure (P_{mn}) for test PG7_3

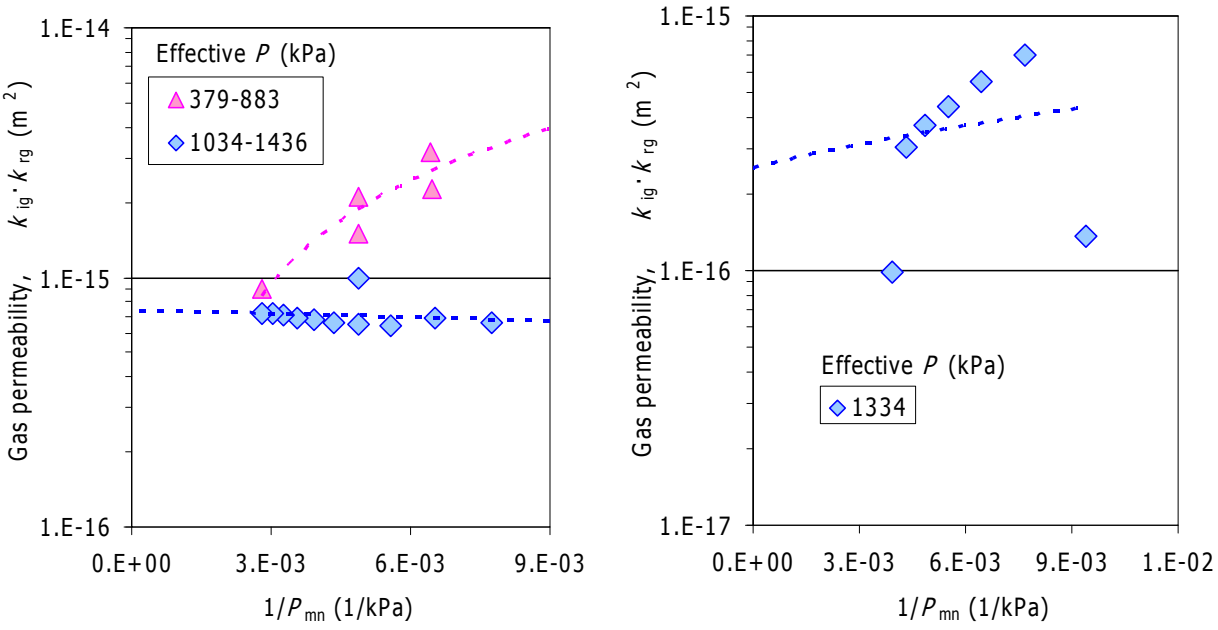

Figure 34: Measured permeability versus inverse of mean pressure (P_{mn}) for tests PG9_2 (left) and PG10_1 (right)

Table III: Average gas permeability values obtained with the steady-state method for different effective pressures and values corrected for the Klinkenberg effect. The values obtained with the unsteady-state method for the same samples are also indicated

Test	ρ_d (g/cm^3)	Final *w* (%)	Effective confining *P* (kPa)	Average $k_{ig}\cdot k_{rg}$ (m^2)	Klinkenberg $k_{ig}\cdot k_{rg}$ (m^2)	Low *P* $k_{ig}\cdot k_{rg}$ (m^2)
PG3_6	2.36	1.6	246-407	$9.1\cdot10^{-17}$	$1.0\cdot10^{-17}$	
PG3_7	2.36	2.2	971-1124	$1.7\cdot10^{-17}$	$1.4\cdot10^{-17}$	$1.2\cdot10^{-16}$
			1146-1363	$1.7\cdot10^{-17}$	$2.0\cdot10^{-17}$	
PG5_6	2.32	1.9	224-558	$1.7\cdot10^{-17}$	$1.3\cdot10^{-17}$	$1.3\cdot10^{-16}$
PG5_8	2.32	0.9	452-754	$8.1\cdot10^{-17}$	$3.3\cdot10^{-17}$	$3.5\cdot10^{-16}$
			892-1347	$3.0\cdot10^{-17}$	$1.9\cdot10^{-17}$	
PG7_3	2.30	1.2	466-967	$5.7\cdot10^{-17}$	$2.4\cdot10^{-17}$	$3.7\cdot10^{-16}$
			1018-1587	$4.9\cdot10^{-17}$	$2.9\cdot10^{-17}$	
PG9_2	2.32	1.1	379-883	$2.0\cdot10^{-15}$		
			1034-1436	$7.1\cdot10^{-16}$	$7.4\cdot10^{-16}$	
PG10_1	2.28	4.0	1334	$3.7\cdot10^{-16}$	$2.5\cdot10^{-16}$	$1.7\cdot10^{-15}$

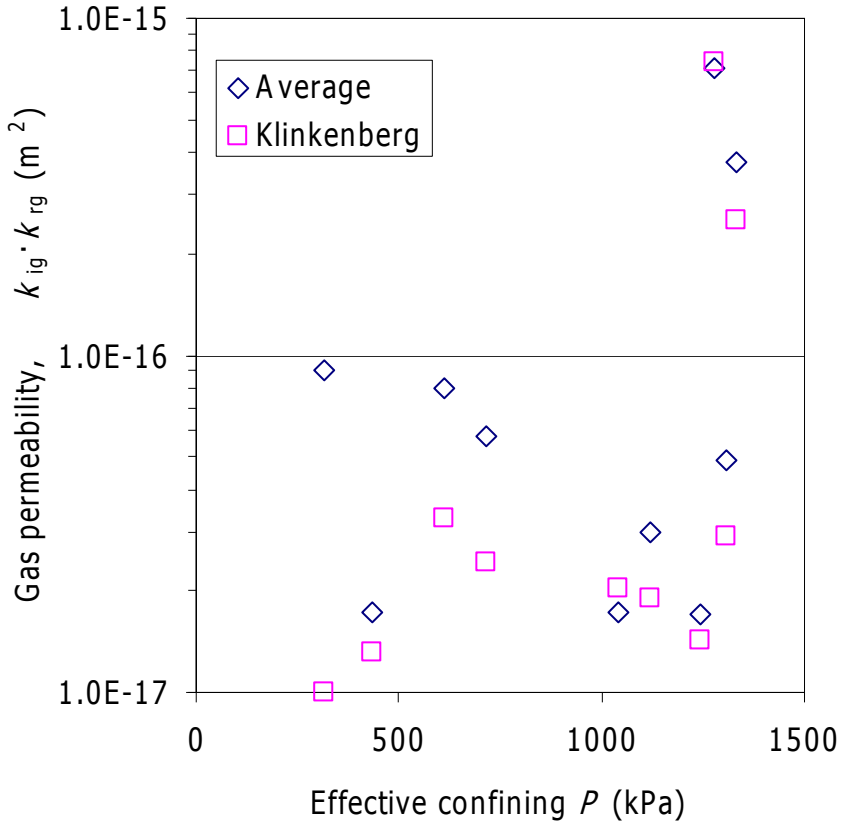

Figure 35: Gas permeability obtained applying different back and injection pressures for different ranges of effective pressure, calculated as an average of all the measurements or applying the Klinkenberg method. The measurements were performed in samples of different water contents and dry densities (Table III)

5.2 INTRINSIC AND RELATIVE PERMEABILITY

The intrinsic permeability depends just on the material characteristics, and its value can be obtained either with a liquid in the saturated material or with gas in the completely dried material, provided that the fluid does not interact with the material. However, if the fluid modifies the characteristics of the material, the value of intrinsic permeability obtained could be altered. The gas permeability measurements performed did not allow to derive the intrinsic permeability, since the specimens were not completely dry. Drying the samples in the oven down to zero water content would have implied modifying their microstructure, and this is why they were just air dried to get different water content values. An indirect method to derive intrinsic permeability from gas permeability measurements was presented in Villar (2002) and Villar & Lloret (2001), and was applied to the measurements shown above.

Figure 13 showed the gas permeability change with water content for samples with different hydraulic history. This parameter presents a better correlation with the permeability values obtained than accessible pore volume or degree of saturation. The following relationship between gas permeability (k_g, m/s) and water content (w, %) could be deduced:

Not previously saturated: $k_g = 3 \cdot 10^{-10} e^{-0.17w}$ [7]

Saturated after air drying: $k_g = 2 \cdot 10^{-10} e^{-0.65w}$ [8]

Previously saturated: $k_g = 1 \cdot 10^{-10} e^{-0.92w}$ [9]

If in these equations the water content is taken as 0, the gas permeability of the dried concrete, which cannot be obtained through direct measurement because of the impossibility of drying completely the samples without modifying their microstructure, would be estimated. Then, the intrinsic permeability of concrete measured with air flow could be obtained through Equation 2, considering k_{rg} equal to 1, since the degree of liquid saturation would be 0. The values thus obtained are shown in Table IV. The intrinsic permeability obtained for the three groups of samples are of the same order of magnitude amongst them and two orders of magnitude higher than the value obtained in saturated samples with water flow ($4 \cdot 10^{-18}$, see section 4.2), what is the expected result, since water reacts with the cement paste and can hydrate the anhydrated cement and change the chemical equilibria by dissolution, leaching and/or precipitation of calcite (if the latter is carbonated). This alteration is probably irreversible, since the gas permeability of previously saturated samples is lower than that of samples not previously saturated. Saturation after air drying implies a slight increase in gas permeability. The gas slippage or Klinkenberg effect is usually invoked as the reason for the difference between gas and water permeabilities but, as shown in the previous section, this effect was not relevant in our tests. Other authors have reached the same conclusion (Loosveldt et al. 2002).

Table IV: Values of gas permeability and of intrinsic permeability deduced with gas flow from the correlations shown in Figure 13 (Equations 7, 8 and 9)

Hydraulic history	k_{g0} (m/s)	k_{ig} (m^2)
Not previously saturated	$3 \cdot 10^{-10}$	$5 \cdot 10^{-16}$
Previously saturated	$1 \cdot 10^{-10}$	$2 \cdot 10^{-16}$
Saturated after air drying	$2 \cdot 10^{-10}$	$3 \cdot 10^{-16}$

If we substitute the intrinsic permeability values of Table IV in Equation 2 for each test (results in Table V to Table XIII) we would obtain the relative gas permeability value for each measurement. The values thus computed are plotted in Figure 36 as a function of the degree of saturation for the different hydraulic histories. The following potential correlations were found:

Not previously saturated: $k_{rg} = 1.2\ S_r^{-0.16}$ [10]

Previously saturated: $k_{rg} = 12.3\ S_r^{-1.24}$ [11]

Saturated after air drying: $k_{rg} = 39.5\ S_r^{-1.46}$ [12]

It is clear that the change of relative gas permeability with degree of saturation is more acute for samples previously saturated, whereas for samples not previously saturated the change of relative gas permeability with degree of saturation is not so significant and the relative gas permeability is distinctly higher for degrees of saturation higher than 20%.

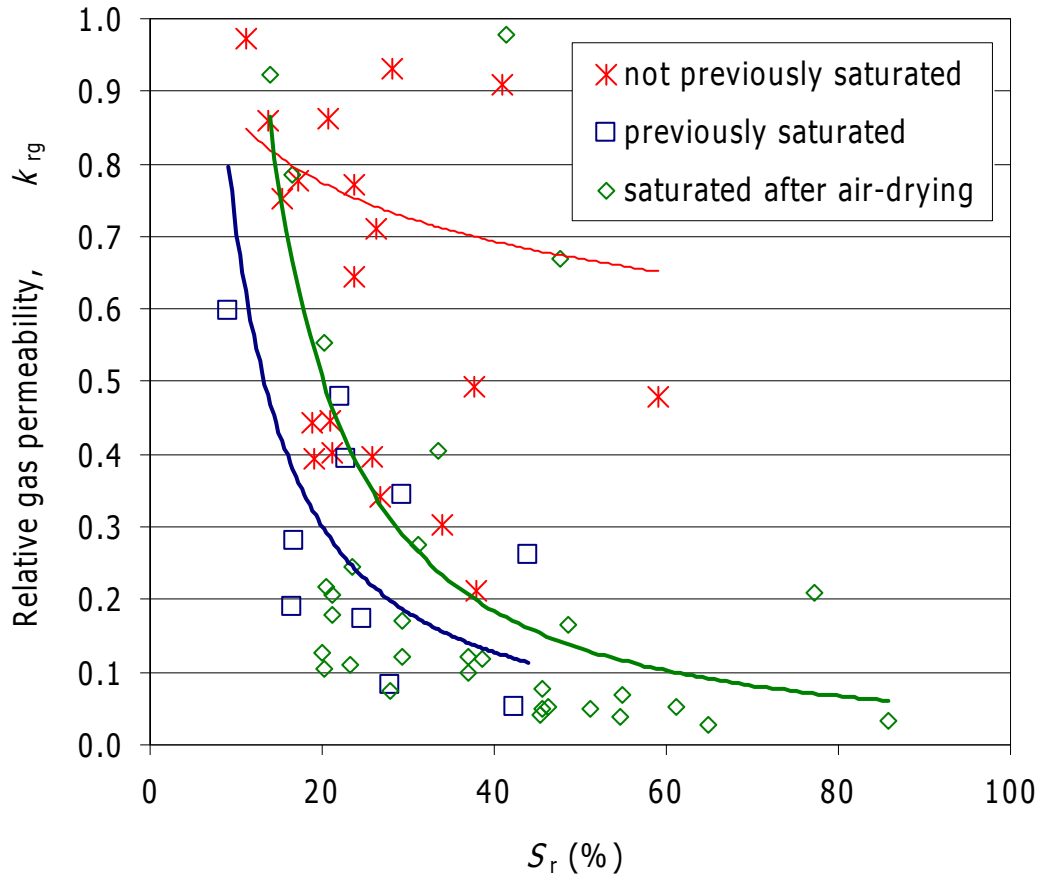

Figure 36: Relative gas permeability of concrete as a function of degree of saturation for different hydraulic histories

It is known that the alkaline composition of the Portland cement matrix renders the cementitious material susceptible to chemical alteration during periods of storage in an unsaturated environment because of drying, carbonation or precipitation within the pore structure. Carbonation modifies the pore network and also the dry mass of the material (Ranaivomanana et al. 2011). This could falsify the initial water contents computed from the dry mass obtained by drying at 110°C at the end of the wetting/drying process.

The drying down to an equilibrium water content at room conditions for the samples used in this study, which had volumes between 40 and 130 cm^3 (Table I), took about 300 days (Figure 12), being faster when the water content was still high. This is usually attributed to the movement of water by capillarity when moisture is high in opposition to the slower diffusion-controlled movement of water for low water contents (Selih et al. 1996).

5.3 ANALYSIS OF MICROCRACKING

Since the gas permeability depends on porosity, microstructure geometry and connectivity of pores, cracking during the drying process prior to gas permeability measurement was also invoked as an additional reason for the differences between gas and liquid water permeabilities (Baroghel-Bouny 2007). However, the modification of the microstructure during drying, with the formation of microcracking by shrinkage, seems to take place just on the surface of concrete, and would not contribute to a faster drying inside the concrete, on the contrary, the moisture would decrease extremely slowly deeper inward (Ryu et al. 2011, Asamato et al. 2011), as the time needed by the samples used in this study to reach an equilibrium water content at room conditions showed. Consequently, during the gas permeability tests, flow could take place preferentially along the potentially altered external surface of the samples.

A certain decrease in gas permeability with confining pressure was observed in the tests performed in the steady-state equipment (Figure 28 and section Analysis of the Klinkenberg effect), particularly for confining pressures above 1000 kPa. Also, the permeability values for the same sample obtained with the unsteady-state method were usually higher than the values obtained with the steady-state method (Table III), in which the confining pressures applied were usually higher. This influence of confining pressure on permeability could suggest the existence of external microcracks, since these would tend to close as the confining pressure increases and the permeability would then be reduced. With the aim of checking if this could be a relevant issue in the tests performed, hydrostatic compression tests in triaxial cells were performed in two samples at the end of the last water permeability test (HOR1s_2 and HOR10s), that is, with the samples saturated. These were samples s1 and s10. In the same triaxial cells in which the water permeability tests were performed (Figure 3), the confining pressure was increased from 100 to 1200 kPa while the pressure on top and bottom of the sample was kept constant at 50 kPa and the water outflow was continuously monitored. The rate of pressure increase was of 60 kPa/h. The unloading ramp was performed at the same speed. Pressure/volume controllers were used to apply both the confining and the backpressures. The change in void ratio of the samples was computed from the water outflow, since the samples were supposed to be initially saturated. The results obtained are shown in Figure 37. A linear relationship between pressure and deformation is expected for non fissured samples, because their compressibility should be constant (for pressures low enough not to cause new fissuring of the sample). In the hydrostatic tests performed the compressibility was higher for confinement pressures below 500 kPa, and seemed to stabilise for higher confining pressures. On the contrary, the effect of confining pressure on permeability, as put forward in Figure 31 to Figure 34, was only noticeable for confining pressures higher than about 1000 kPa. Consequently, no clear conclusion could be drawn from these tests with respect to microcracking being responsible of the effect of confining pressure on permeability, although it cannot be ruled out.

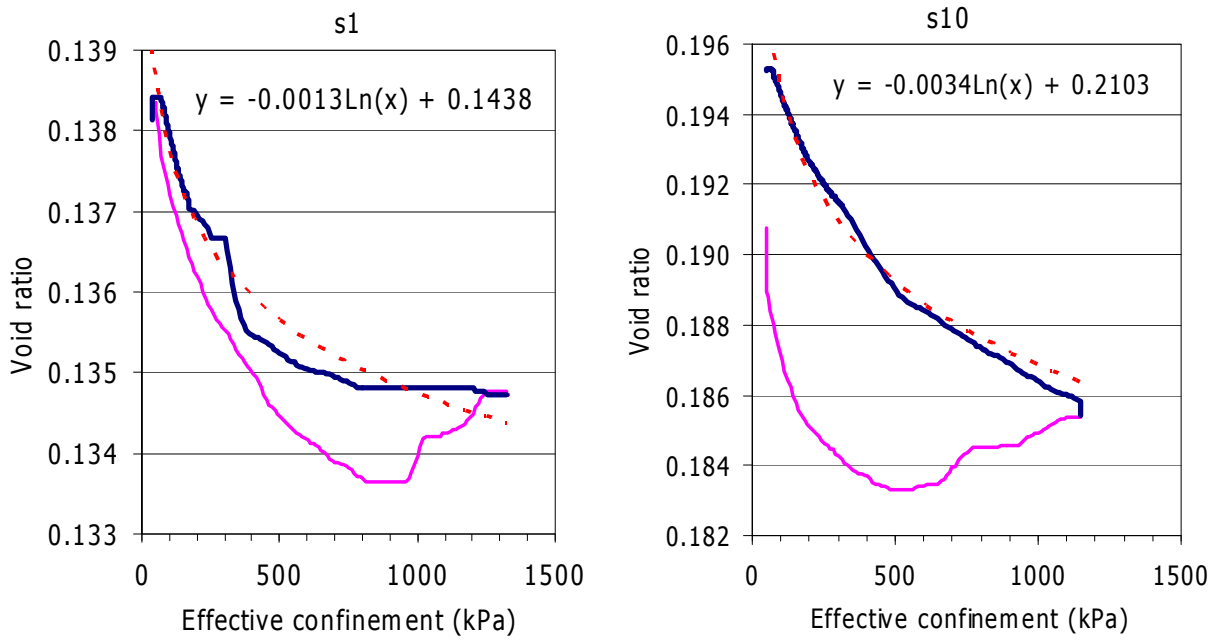

Figure 37: Hydrostatic compression tests performed in concrete samples 1 and 10

Conclusions

In order to perform the hydraulic characterisation of concrete, particularly with respect to its gas (nitrogen) transport properties, a steady-state setup for the measurement of gas permeability of concrete with different degrees of saturation under different pressure conditions was fine tuned. The gas pressure of the samples was also measured in an unsteady-state equipment working under low injection pressures. These measurements allowed the estimation of the intrinsic and relative gas permeability of the concrete.

Permeability decreased with water content, but it was also greatly affected by the hydraulic history of concrete, *i.e*. if it had been previously dried or wetted. In particular, and for a given degree of saturation, the gas permeability of concrete previously saturated was lower than if the concrete had been just air dried or saturated after air drying. In any case, the gas permeability was about two orders of magnitude higher than the liquid water permeability (10^{-16} *vs*. 10^{-18} m^2), probably due to the chemical reactions taking place during saturation (carbonation). The relative gas permeability of concrete increased sharply for water degrees of saturation smaller than 50%.

The slowness of the processes occurring in concrete was illustrated by the time needed by the samples to get equilibrium water contents under room conditions and to reach a constant permeability value when they were saturated.

Also, the boundary conditions affected the gas permeability values, and thus, they seemed to be mostly conditioned by the backpressure and the confining pressure, increasing as the former increased and decreasing as the latter increased, *i.e*. decreasing as the effective pressure increased. Overall the increase of pressure head or injection pressure implied a decrease in gas permeability, although this effect was less significant when the pressure head was high. Consequently, all the values obtained with the unsteady-state equipment were higher than those obtained with the steady-state one, in which the confining and injection pressures applied were higher. Although microcracking during air-drying could not be ruled out as

responsible for the decrease of permeability with confining pressure, the hydrostatic tests performed did not clearly confirm this hypothesis.

The apparent permeability was calculated applying the Klinkenberg method to the results obtained with the steady-state equipment. The permeability thus obtained for a given effective confining pressure was only slightly smaller (by an average factor of 1.5) than the average of all the values measured for the same confining pressure range. For this reason it is considered that the Klinkenberg effect was not relevant in the range of pressures applied.

The behaviour observed, in particular concerning hysteresis, highlighted the importance of microstructural analyses to understand the hydraulic properties of concrete.

Acknowledgements

The research leading to these results received funding from the European Atomic Energy Community's Seventh Framework Programme (FP7/2007-2011) under Grant Agreement n°230357, the FORGE project. This work was additionally financed by ENRESA through a CIEMAT-ENRESA General Agreement. The laboratory work was performed by Ramón Campos and Juan Aroz, from CIEMAT.

References

ASAMATO, S., OHTSUKA, A., KUWAHAR, Y., MIURA, C. 2011. Study of the effects of solar radiation and rain on shrinkage, shrinkage cracking and creep of concrete. *Cement and Concrete Research* 41, 590-601.

BAROGHEL-BOUNY, V. 2007. Water vapour sorption experiments on hardened cementitious materials. Part II: Essential tool for assesmente of transport properties and for durability prediction. *Cement and Concrete Research* 37, 438-454.

LLORET, A. 1982. *Comportamiento deformacional del suelo no saturado bajo condiciones drenadas y no drenadas*. Ph. D. Thesis. Universidad Politécnica de Cataluña.

LOOSVELDT, H., LAFHAJ, Z., SKOCZYLAS, F. 2002. Experimental study of gas and liquid permeability of a mortar. *Cement and Concrete Research* 32(9), 1357-1363.

RANAIVOMANANA, H., VERDIER, J., SELLIER, A., BOURBON, X. 2011. Toward a better comprehension and modelling of hysteresis cycles in the water sorption-desorption process for cement based materials. *Cement and Concrete Research* 41, 817-827.

RYU, D.W., KO, J.W., NOGUCHI, T. 2011. Effects of simulated environmental conditions on the internal relative humidity and relative moisture content distribution of exposed concrete. *Cement and Concrete Research* 33, 142-153.

SCHEIDEGGER, A.E. 1974. *The physics of flow through porous media*. 3rd ed. Toronto: University of Toronto Press, 353 pp.

SELIH, J., SOUSA, A.C.M., BREMNER, T.W. 1996. Moisture transport of initially fully saturated concrete during drying. *Transport in Porous Media* 24, 81-106.

VILLAR, M.V., 2002. Thermo-hydro-mechanical characterisation of a bentonite from Cabo de Gata. A study applied to the use of bentonite as sealing material in high level radioactive waste repositories. *Publicación Técnica ENRESA* 01/2002, Madrid, 258 pp.

VILLAR, M.V., LLORET, A., 2001. Variation of the intrinsic permeability of expansive clay upon saturation. 259-266 in *Clay Science for Engineering*. ADACHI, K. & FUKUE, M. (editors), Rotterdam: Balkema. ISBN 90 5809 175 9.

VILLAR, M.V., MARTÍN, P.L., BARCALA, J.M. 2009. Caracterización del material de cobertera y el hormigón del C. A. El Cabril. Caracterización termo-hidro-mecánica. *Informe Técnico* CIEMAT/DMA/2G205/03/09. Madrid, 55 pp. Agosto 2009.

VILLAR, M.V.; MARTÍN, P.L., BARCALA, J.M. 2010. Description of experimental setups and procedures for CIEMAT gas transport tests of WP3. *Informe Técnico* CIEMAT/DMA/2G207/01/10, Madrid, 13 pp.

YOSHIMI, Y., OSTERBERG, J.O. 1963. Compression of partially saturated cohesive soils. *J. Soil Mechanics and Foundations Division*. ASCE 89, SM 4, 1-24.

ZULOAGA, P. 2008. Modelo de comportamiento de barreras de hormigón para el aislamiento de residuos radiactivos de baja actividad. *Publicación Técnica ENRESA* 02/2008. Madrid, 237 pp.

Appendix 1

DATA OF MEASUREMENTS WITH THE UNSTEADY-STATE METHOD

Table V: Results of gas permeability measurements during air drying in sample 1 before and after saturation (ρ_d=2.31 g/cm^3, *e*=0.16)

Test	Drying (days)	*T* (°C)	*w* final (%)	S_r final (%)	$k_{ig}{\cdot}k_{rg}$ (m^2)	*e* (1-S_r)	k_g (m/s)
PG1_1	206	24	0.8	55	$5.1{\cdot}10^{-16}$	0.07	$3.1{\cdot}10^{-10}$
PG1_2 [a]	211	22	2.3	38	$2.4{\cdot}10^{-16}$	0.10	$1.5{\cdot}10^{-10}$
PG1_3	240	22	1.6	26	$3.5{\cdot}10^{-16}$	0.12	$2.1{\cdot}10^{-10}$
PG1_4	260	25	1.4	24	$3.1{\cdot}10^{-16}$	0.12	$1.9{\cdot}10^{-10}$
PG1_5	304	24	1.4	24	$3.7{\cdot}10^{-16}$	0.12	$2.3{\cdot}10^{-10}$
PG1_6	336	24	1.3	21	$4.2{\cdot}10^{-16}$	0.13	$2.6{\cdot}10^{-10}$
PG1_7	398	21	1.1	17	$3.8{\cdot}10^{-16}$	0.13	$2.3{\cdot}10^{-10}$
PG1_8	485	21	0.8	14	$4.2{\cdot}10^{-16}$	0.14	$2.6{\cdot}10^{-10}$
PG1_9	785	21	0.7	11	$4.7{\cdot}10^{-16}$	0.14	$2.9{\cdot}10^{-10}$
After saturation (HOR1s)							
PG1_10	3	23	3.3	55	$2.3{\cdot}10^{-17}$	0.07	$1.4{\cdot}10^{-11}$
PG1_11	39	26	2.8	45	$1.4{\cdot}10^{-17}$	0.09	$8.5{\cdot}10^{-12}$
PG1_12	88	25	2.2	37	$3.2{\cdot}10^{-17}$	0.10	$2.0{\cdot}10^{-11}$
PG1_13	103	25	2.2	37	$3.9{\cdot}10^{-17}$	0.10	$2.4{\cdot}10^{-11}$
PG1_14	139	24	1.8	29	$5.5{\cdot}10^{-17}$	0.12	$3.4{\cdot}10^{-11}$
PG1_15	178	21	1.8	29	$4.0{\cdot}10^{-17}$	0.11	$2.4{\cdot}10^{-11}$
PG1_16	301	24	1.3	21	$5.8{\cdot}10^{-17}$	0.13	$3.6{\cdot}10^{-11}$
PG1_17	399	23	1.2	20	$7.1{\cdot}10^{-17}$	0.13	$4.4{\cdot}10^{-11}$

[a] The sample got accidentally wet at the end of the first measurement and it was dried at 60°C

Table VI: Results of gas permeability measurements in sample 2 during air drying before and after saturation (ρ_d=2.32 g/cm^3, *e*=0.16)

Test	Drying (days)	*T* (°C)	*w* final (%)	S_r final (%)	$k_{ig}{\cdot}k_{rg}$ (m^2)	*e* (1-S_r)	k_g (m/s)
PG2_1	8	24	3.3	57	$5.8{\cdot}10^{-16}$	0.07	$3.6{\cdot}10^{-10}$
PG2_2	33	25	2.4	40	$7.1{\cdot}10^{-16}$	0.09	$4.4{\cdot}10^{-10}$
PG2_3	54	23	2.0	35	$7.4{\cdot}10^{-16}$	0.10	$4.5{\cdot}10^{-10}$
PG2_4	102	25	2.4	41	$4.4{\cdot}10^{-16}$	0.09	$2.7{\cdot}10^{-10}$
PG2_5	168	21	1.8	30	$7.3{\cdot}10^{-16}$	0.11	$4.5{\cdot}10^{-10}$
PG2_6	197	23	1.4	23	$8.0{\cdot}10^{-16}$	0.12	$5.0{\cdot}10^{-10}$
PG2_7	273	23	1.0	18	$9.0{\cdot}10^{-16}$	0.13	$5.6{\cdot}10^{-10}$

Test	Drying (days)	*T* (°C)	*w* final (%)	S_r final (%)	$k_{ig} \cdot k_{rg}$ (m^2)	*e* (1-S_r)	k_g (m/s)
After saturation (HOR2s)							
PG2_8	3	22	3.4	58	$3.4 \cdot 10^{-16}$	0.07	$2.1 \cdot 10^{-10}$
PG2_9	10	19	3.1	53	$3.8 \cdot 10^{-16}$	0.07	$2.3 \cdot 10^{-10}$
PG2_10	21	21	2.5	43	$3.7 \cdot 10^{-16}$	0.09	$2.3 \cdot 10^{-10}$

Table VII: Results of gas permeability measurements in sample 3s after saturation and air drying and then during air drying after resaturation (ρ_d=2.36 g/cm^3, *e*=0.14)

Test	Drying (days)	*T* (°C)	*w* final (%)	S_r final (%)	$k_{ig} \cdot k_{rg}$ (m^2)	*e* (1-S_r)	k_g (m/s)
PG3_1	123	20	1.5	29	$5.6 \cdot 10^{-17}$	0.10	$3.4 \cdot 10^{-11}$
PG3_2	201	22	1.2	23	$6.4 \cdot 10^{-17}$	0.11	$3.9 \cdot 10^{-11}$
PG3_3	299	22	0.9	17	$4.6 \cdot 10^{-17}$	0.11	$2.8 \cdot 10^{-11}$
PG3_4	424	25	0.5	9	$9.7 \cdot 10^{-17}$	0.12	$6.0 \cdot 10^{-11}$
PG3_5 [a]	462	17	1.1	22	$7.8 \cdot 10^{-17}$	0.11	$4.8 \cdot 10^{-11}$
PG3_6 [a]	543	21	0.6	12	$2.1 \cdot 10^{-16}$	0.12	$1.3 \cdot 10^{-10}$
PG3_7	838	20	0.9	17	$1.2 \cdot 10^{-16}$	0.11	$7.2 \cdot 10^{-11}$
PG3_8	925	18	2.2	44	$4.2 \cdot 10^{-17}$	0.08	$2.6 \cdot 10^{-11}$
After resaturation (HOR3s_2)							
PG3_9	14	22	3.9	76	no flow	0.03	
PG3_10	24	22	4.0	86	$7.8 \cdot 10^{-18}$	0.02	$4.8 \cdot 10^{-12}$
PG3_13	91	21	2.6	55	$1.1 \cdot 10^{-17}$	0.06	$6.8 \cdot 10^{-12}$
PG3_14	118	21	2.0	43	$1.3 \cdot 10^{-17}$	0.06	$7.8 \cdot 10^{-12}$
PG3_15	138	25	2.5	51	$2.5 \cdot 10^{-18}$	0.08	$1.6 \cdot 10^{-12}$
PG3_16	173	23	2.1	46	$1.6 \cdot 10^{-17}$	0.07	$1.0 \cdot 10^{-11}$
PG3_18	364	22	1.5	25	$1.6 \cdot 10^{-17}$	0.07	$9.7 \cdot 10^{-12}$

[a] The sample got accidentally wet after the test

Table VIII: Results of the gas permeability measurements in sample 4s after saturation and air drying and then during air drying after resaturation (ρ_d=2.33 g/cm^3, *e*=0.15)

Test	Drying (days)	*T* (°C)	*w* final (%)	S_r final (%)	$k_{ig} \cdot k_{rg}$ (m^2)	*e* (1-S_r)	k_g (m/s)
PG4_1	316	22	1.5	28	$1.8 \cdot 10^{-15}$	0.11	$1.1 \cdot 10^{-9}$
After resaturation (HOR4s_2)							
PG4_2	3	28	4.3	77	$6.8 \cdot 10^{-17}$	0.03	$4.2 \cdot 10^{-11}$
PG4_3	25	24	2.3	41	$3.2 \cdot 10^{-16}$	0.09	$2.0 \cdot 10^{-10}$
PG4_4	40	23	1.9	33	$4.7 \cdot 10^{-16}$	0.10	$2.9 \cdot 10^{-10}$
PG4_5	418	25	1.6	29	$6.2 \cdot 10^{-16}$	0.11	$3.8 \cdot 10^{-10}$

Test	Drying (days)	*T* (°C)	*w* final (%)	S_r final (%)	$k_{ig} \cdot k_{rg}$ (m^2)	*e* (1-S_r)	k_g (m/s)
PG4_7	164	20	1.2	21	$9.0 \cdot 10^{-16}$	0.12	$5.5 \cdot 10^{-10}$

Table IX: Results of the gas permeability measurements in samples 5s after saturation and air drying and then during air drying after resaturation (ρ_d=2.32 g/cm^3, *e*=0.16)

Test	Drying (days)	*T* (°C)	*w* final (%)	S_r final (%)	$k_{ig} \cdot k_{rg}$ (m^2)	*e* (1-S_r)	k_g (m/s)
PG5_1	3	22	2.4	28	$1.3 \cdot 10^{-17}$	0.11	$8.3 \cdot 10^{-12}$
PG5_2	30	23	2.5	42	$1.7 \cdot 10^{-17}$	0.09	$1.0 \cdot 10^{-11}$
PG5_3	98	24	1.4	25	$5.6 \cdot 10^{-17}$	0.12	$3.5 \cdot 10^{-11}$
PG5_4	156	21	1.0	17	$6.2 \cdot 10^{-17}$	0.13	$3.8 \cdot 10^{-11}$
After resaturation (HOR5s_2)							
PG5_6	26	24	1.9	34	$1.3 \cdot 10^{-16}$	0.10	$8.1 \cdot 10^{-11}$
PG5_7	95	26	0.8	14	$3.0 \cdot 10^{-16}$	0.13	$1.8 \cdot 10^{-10}$
PG5_8	250	21	0.9	15	$3.5 \cdot 10^{-16}$	0.13	$2.2 \cdot 10^{-10}$
After resaturation (HOR5s_3)							
PG5_10	76	21	2.7	46	$1.7 \cdot 10^{-17}$	0.08	$1.1 \cdot 10^{-11}$
PG5_11	125	23	1.3	23	$3.5 \cdot 10^{-17}$	0.12	$2.2 \cdot 10^{-11}$
PG5_12[a]	268	22	1.2	20	$3.4 \cdot 10^{-17}$	0.12	$2.1 \cdot 10^{-11}$
PG5_14	628	23	1.4	24	$7.9 \cdot 10^{-17}$	0.12	$4.9 \cdot 10^{-11}$

[a] The sample got accidentally wet at the end of this test

Table X: Results of gas permeability measurements in sample 6s after saturation and air drying and then during air drying after resaturation (ρ_d=2.32 g/cm^3, *e*=0.15)

Test	Drying (days)	*T* (°C)	*w* final (%)	S_r final (%)	$k_{ig} \cdot k_{rg}$ (m^2)	*e* (1-S_r)	k_g (m/s)
PG6_1	158	25	0.9	16	$1.3 \cdot 10^{-16}$	0.13	$7.8 \cdot 10^{-11}$
PG6_2	623	22	0.9	15	$7.3 \cdot 10^{-16}$	0.13	$4.5 \cdot 10^{-10}$
After resaturation (HOR6s_2)							
PG6_3	5	20	2.9	48	$1.1 \cdot 10^{-16}$	0.08	$6.7 \cdot 10^{-11}$
PG6_4	77	22	1.2	20	$1.8 \cdot 10^{-16}$	0.12	$1.1 \cdot 10^{-10}$
PG6_5	336	23	1.1	18	$4.6 \cdot 10^{-16}$	0.13	$2.8 \cdot 10^{-10}$
PG6_6	587	22	1.1	18	$4.2 \cdot 10^{-16}$	0.13	$2.6 \cdot 10^{-10}$

Table XI: Results of gas permeability measurements in sample 7 during air drying and then during air drying after saturation (ρ_d=2.30 g/cm^3, *e*=0.16)

Test	Drying (days)	*T* (°C)	*w* final (%)	S_r final (%)	$k_{ig}\cdot k_{rg}$ (m^2)	*e* (1-S_r)	k_g (m/s)
PG7_1	20	24	3.6	59	$2.3\cdot10^{-16}$	0.07	$1.4\cdot10^{-10}$
PG7_2	36	24	1.7	28	$4.5\cdot10^{-16}$	0.12	$2.8\cdot10^{-10}$
PG7_3	62	26	0.9	15	$3.6\cdot10^{-16}$	0.14	$2.2\cdot10^{-10}$
After saturation (HOR7s)							
PG7_4	4	23	3.6	61	$1.7\cdot10^{-17}$	0.06	$1.0\cdot10^{-11}$
PG7_5	25	27	2.7	46	$2.5\cdot10^{-17}$	0.09	$1.5\cdot10^{-11}$
PG7_6	56	24	1.7	28	$2.4\cdot10^{-17}$	0.12	$1.5\cdot10^{-11}$
PG7_7	182	23	1.3	21	$6.7\cdot10^{-17}$	0.13	$4.1\cdot10^{-11}$
PG7_8	303	22	1.2	20	$4.1\cdot10^{-17}$	0.13	$2.5\cdot10^{-11}$

Table XII: Results of gas permeability measurements in sample 9 during air drying and then during air drying after saturation (ρ_d=2.32 g/cm^3, *e*=0.15)

Test	Drying (days)	*T* (°C)	*w* final (%)	S_r final (%)	$k_{ig}\cdot k_{rg}$ (m^2)	*e* (1-S_r)	k_g (m/s)
PG9_3	344	24	0.8	14	$1.1\cdot10^{-15}$	0.13	$7.1\cdot10^{-10}$
After saturation (HOR9s)							
PG9_4	3	23	3.9	65	$8.7\cdot10^{-18}$	0.05	$5.4\cdot10^{-12}$
PG9_5	18	26	2.9	49	$5.3\cdot10^{-17}$	0.08	$3.3\cdot10^{-11}$
PG9_6	39	24	2.4	39	$3.8\cdot10^{-17}$	0.09	$2.3\cdot10^{-11}$
PG9_7	135	20	1.8	31	$8.9\cdot10^{-17}$	0.11	$5.5\cdot10^{-11}$

Table XIII: Results of gas permeability measurements in sample 10 during air drying and then during air drying after saturation (ρ_d=2.28 g/cm^3, *e*=0.18)

Test	Drying (days)	*T* (°C)	*w* final (%)	S_r final (%)	$k_{ig}\cdot k_{rg}$ (m^2)	*e* (1-S_r)	k_g (m/s)
PG10_1	48	21	4.0	60	$1.7\cdot10^{-15}$	0.07	$1.0\cdot10^{-9}$
PG10_3	154	24	2.5	38	$1.0\cdot10^{-16}$	0.11	$6.4\cdot10^{-11}$
PG10_4	168	24	2.2	34	$1.5\cdot10^{-16}$	0.12	$9.1\cdot10^{-11}$
PG10_5	206	25	1.7	27	$1.7\cdot10^{-16}$	0.13	$1.0\cdot10^{-10}$
PG10_6	231	24	1.4	21	$2.0\cdot10^{-16}$	0.14	$1.2\cdot10^{-10}$
PG10_7	400	21	1.2	19	$2.2\cdot10^{-16}$	0.14	$1.3\cdot10^{-10}$
PG10_8	427	21	1.4	21	$2.2\cdot10^{-16}$	0.14	$1.3\cdot10^{-10}$
PG10_9	463	22	1.1	19	$1.9\cdot10^{-16}$	0.14	$1.2\cdot10^{-10}$
PG10_10	689	21	1.1	26	$1.9\cdot10^{-16}$	0.13	$1.2\cdot10^{-10}$

DATA OF MEASUREMENTS WITH THE STEADY-STATE METHOD

Table XIV: Results of gas permeability measurements in sample 3 (test PG3_6) obtained with the steady-state method (ρ_d=2.36 g/cm^3, *w*=1.6%)

Duration (days)	Confining *P* (kPa)	Injection *P* (kPa)	Back *P* (kPa)	$k_{ig}\cdot k_{rg}$ inflow (m^2)	$k_{ig}\cdot k_{rg}$ outflow (m^2)	k_g inflow (m/s)	k_g outflow (m/s)
3	401	210	100	$9.1\cdot10^{-17}$	$1.0\cdot10^{-16}$	$1.2\cdot10^{-10}$	$6.3\cdot10^{-11}$
3	413	200	100	$8.4\cdot10^{-17}$	$1.1\cdot10^{-16}$	$1.0\cdot10^{-10}$	$7.0\cdot10^{-11}$
3	449	220	101	$8.0\cdot10^{-17}$	$8.8\cdot10^{-17}$	$1.1\cdot10^{-10}$	$5.4\cdot10^{-11}$
1	450	150	100	$8.5\cdot10^{-17}$	$1.1\cdot10^{-16}$	$7.8\cdot10^{-11}$	$6.6\cdot10^{-11}$
1	451	160	100	$8.2\cdot10^{-17}$	$9.9\cdot10^{-17}$	$8.1\cdot10^{-11}$	$6.1\cdot10^{-11}$
2	549	300	100	$6.5\cdot10^{-17}$	$6.9\cdot10^{-17}$	$1.2\cdot10^{-10}$	$4.3\cdot10^{-11}$
4	650	401	85	$5.7\cdot10^{-17}$	$5.9\cdot10^{-17}$	$1.4\cdot10^{-10}$	$3.1\cdot10^{-11}$

Table XV: Results of gas permeability measurements in sample 3 (test PG3_7) obtained with the steady-state method (ρ_d=2.36 g/cm^3, *w*=2.2%)

Duration (h)	Confining *P* (kPa)	Injection *P* (kPa)	Back *P* (kPa)	$k_{ig}\cdot k_{rg}$ inflow (m^2)	$k_{ig}\cdot k_{rg}$ outflow (m^2)	k_g inflow (m/s)	k_g outflow (m/s)
4.0	1519	200	110	$1.90\cdot10^{-17}$	$1.84\cdot10^{-17}$	$2.4\cdot10^{-11}$	$1.3\cdot10^{-11}$
16.0	1503	300	110	$1.81\cdot10^{-17}$	$1.81\cdot10^{-17}$	$3.4\cdot10^{-11}$	$1.2\cdot10^{-11}$
2.7	1500	400	110	$1.71\cdot10^{-17}$	$1.74\cdot10^{-17}$	$4.2\cdot10^{-11}$	$1.2\cdot10^{-11}$
1.5	1502	500	110	$1.65\cdot10^{-17}$	$1.67\cdot10^{-17}$	$5.1\cdot10^{-11}$	$1.1\cdot10^{-11}$
1.3	1504	600	110	$1.68\cdot10^{-17}$	$1.65\cdot10^{-17}$	$6.3\cdot10^{-11}$	$1.1\cdot10^{-11}$
0.8	1506	700	110	$1.70\cdot10^{-17}$	$1.65\cdot10^{-17}$	$7.4\cdot10^{-11}$	$1.1\cdot10^{-11}$
1.0	1506	800	110	$1.70\cdot10^{-17}$	$1.67\cdot10^{-17}$	$8.4\cdot10^{-11}$	$1.1\cdot10^{-11}$
67.2	1529	900	110	$1.77\cdot10^{-17}$	$1.74\cdot10^{-17}$	$9.8\cdot10^{-11}$	$1.2\cdot10^{-11}$
1.1	1528	1000	110	$1.81\cdot10^{-17}$	$1.78\cdot10^{-17}$	$1.1\cdot10^{-10}$	$1.2\cdot10^{-11}$
0.7	1529	900	110	$1.74\cdot10^{-17}$	$1.76\cdot10^{-17}$	$9.7\cdot10^{-11}$	$1.2\cdot10^{-11}$
1.9	1530	800	110	$1.76\cdot10^{-17}$	$1.74\cdot10^{-17}$	$8.7\cdot10^{-11}$	$1.2\cdot10^{-11}$
1.3	1530	700	110	$1.70\cdot10^{-17}$	$1.73\cdot10^{-17}$	$7.4\cdot10^{-11}$	$1.2\cdot10^{-11}$
41.7	1518	600	110	$1.56\cdot10^{-17}$	$1.58\cdot10^{-17}$	$5.8\cdot10^{-11}$	$1.0\cdot10^{-11}$
1.4	1518	500	110	$1.58\cdot10^{-17}$	$1.63\cdot10^{-17}$	$4.9\cdot10^{-11}$	$1.1\cdot10^{-11}$
2.2	1521	400	110	$1.68\cdot10^{-17}$	$1.70\cdot10^{-17}$	$4.2\cdot10^{-11}$	$1.2\cdot10^{-11}$
3.3	1523	300	110	$1.59\cdot10^{-17}$	$1.77\cdot10^{-17}$	$3.0\cdot10^{-11}$	$1.2\cdot10^{-11}$
18.5	556	200	110	$3.16\cdot10^{-17}$	$3.51\cdot10^{-17}$	$4.0\cdot10^{-11}$	$2.3\cdot10^{-11}$

Duration (h)	Confining *P* (kPa)	Injection *P* (kPa)	Back *P* (kPa)	$k_{ig}\cdot k_{rg}$ inflow (m^2)	$k_{ig}\cdot k_{rg}$ outflow (m^2)	k_g inflow (m/s)	k_g outflow (m/s)
1.1	634	300	110	$2.85\cdot10^{-17}$	$3.12\cdot10^{-17}$	$5.3\cdot10^{-11}$	$2.1\cdot10^{-11}$
4.9	725	300	110	$2.65\cdot10^{-17}$	$2.82\cdot10^{-17}$	$4.9\cdot10^{-11}$	$1.9\cdot10^{-11}$
16.3	730	400	110	$2.86\cdot10^{-17}$	$2.92\cdot10^{-17}$	$7.1\cdot10^{-11}$	$2.0\cdot10^{-11}$
0.3	821	400	110	$2.69\cdot10^{-17}$	$2.68\cdot10^{-17}$	$6.7\cdot10^{-11}$	$1.8\cdot10^{-11}$
1.0	831	500	110	$2.73\cdot10^{-17}$	$2.74\cdot10^{-17}$	$8.5\cdot10^{-11}$	$1.9\cdot10^{-11}$
1.7	932	500	110	$2.49\cdot10^{-17}$	$2.48\cdot10^{-17}$	$7.7\cdot10^{-11}$	$1.7\cdot10^{-11}$
71.0	1019	600	110	$2.23\cdot10^{-17}$	$2.26\cdot10^{-17}$	$8.3\cdot10^{-11}$	$1.5\cdot10^{-11}$
1.1	1020	700	110	$2.36\cdot10^{-17}$	$2.35\cdot10^{-17}$	$1.0\cdot10^{-10}$	$1.5\cdot10^{-11}$
0.6	1126	700	110	$2.11\cdot10^{-17}$	$2.15\cdot10^{-17}$	$9.2\cdot10^{-11}$	$1.4\cdot10^{-11}$
1.6	1128	800	110	$2.27\cdot10^{-17}$	$2.24\cdot10^{-17}$	$1.1\cdot10^{-10}$	$1.5\cdot10^{-11}$
1.4	1235	900	110	$2.16\cdot10^{-17}$	$2.15\cdot10^{-17}$	$1.2\cdot10^{-10}$	$1.4\cdot10^{-11}$
0.5	1324	900	110	$2.03\cdot10^{-17}$	$2.00\cdot10^{-17}$	$1.1\cdot10^{-10}$	$1.3\cdot10^{-11}$
0.5	1325	1000	110	$2.12\cdot10^{-17}$	$2.10\cdot10^{-17}$	$1.3\cdot10^{-10}$	$1.4\cdot10^{-11}$
0.4	1529	1000	110	$1.82\cdot10^{-17}$	$1.79\cdot10^{-17}$	$1.1\cdot10^{-10}$	$1.2\cdot10^{-11}$

Table XVI: Results of gas permeability measurements in sample 5 (test PG5_6) obtained with the steady-state method (ρ_d=2.32 g/cm^3, *w*=1.9%)

Duration (days)	Confining *P* (kPa)	Injection *P* (kPa)	Back *P* (kPa)	$k_{ig}\cdot k_{rg}$ inflow (m^2)	$k_{ig}\cdot k_{rg}$ outflow (m^2)	k_g inflow (m/s)	k_g outflow (m/s)
Phase 1							
5	719	300	174	$2.1\cdot10^{-17}$	$2.3\cdot10^{-17}$	$3.8\cdot10^{-11}$	$2.4\cdot10^{-11}$
1	716	401	174	$1.9\cdot10^{-17}$	$1.1\cdot10^{-17}$	$4.8\cdot10^{-11}$	$1.2\cdot10^{-11}$
1	716	501	174	$2.1\cdot10^{-17}$	$2.2\cdot10^{-17}$	$6.4\cdot10^{-11}$	$2.3\cdot10^{-11}$
1	713	601	174	$3.6\cdot10^{-17}$	$3.7\cdot10^{-17}$	$1.3\cdot10^{-10}$	$3.9\cdot10^{-11}$
1	994	700	174	$1.6\cdot10^{-17}$	$1.7\cdot10^{-17}$	$7.0\cdot10^{-11}$	$1.9\cdot10^{-11}$
Phase 2							
3	999	800	174	$2.5\cdot10^{-17}$	$2.6\cdot10^{-17}$	$1.2\cdot10^{-10}$	$2.8\cdot10^{-11}$
1	999	800	273	$1.7\cdot10^{-17}$	$1.7\cdot10^{-17}$	$8.4\cdot10^{-11}$	$2.9\cdot10^{-11}$
1	999	800	374	$1.7\cdot10^{-17}$	$1.7\cdot10^{-17}$	$8.2\cdot10^{-11}$	$3.8\cdot10^{-11}$
1	999	800	435	$1.6\cdot10^{-17}$	$1.6\cdot10^{-17}$	$8.0\cdot10^{-11}$	$4.3\cdot10^{-11}$
<1	999	800	474	$1.6\cdot10^{-17}$	$1.6\cdot10^{-17}$	$8.0\cdot10^{-11}$	$4.7\cdot10^{-11}$
1	999	800	574	$1.6\cdot10^{-17}$	$1.5\cdot10^{-17}$	$7.8\cdot10^{-11}$	$5.5\cdot10^{-11}$
<1	999	800	670	$1.6\cdot10^{-17}$	$1.3\cdot10^{-17}$	$7.8\cdot10^{-11}$	$5.4\cdot10^{-11}$
<1	999	800	749	$1.6\cdot10^{-17}$	$1.2\cdot10^{-17}$	$7.9\cdot10^{-11}$	$5.7\cdot10^{-11}$

Duration (days)	Confining *P* (kPa)	Injection *P* (kPa)	Back *P* (kPa)	$k_{ig}\cdot k_{rg}$ inflow (m^2)	$k_{ig}\cdot k_{rg}$ outflow (m^2)	k_g inflow (m/s)	k_g outflow (m/s)
<1	999	800	648	$1.6\cdot10^{-17}$	$1.5\cdot10^{-17}$	$7.9\cdot10^{-11}$	$6.1\cdot10^{-11}$
1	999	800	550	$1.5\cdot10^{-17}$	$1.5\cdot10^{-17}$	$7.6\cdot10^{-11}$	$5.2\cdot10^{-11}$
1	999	800	349	$1.5\cdot10^{-17}$	$1.6\cdot10^{-17}$	$7.5\cdot10^{-11}$	$3.5\cdot10^{-11}$
<1	999	800	299	$1.4\cdot10^{-17}$	$1.4\cdot10^{-17}$	$7.1\cdot10^{-11}$	$2.6\cdot10^{-11}$
1	999	800	250	$1.5\cdot10^{-17}$	$1.5\cdot10^{-17}$	$7.4\cdot10^{-11}$	$2.4\cdot10^{-11}$
<1	999	800	200	$1.5\cdot10^{-17}$	$1.6\cdot10^{-17}$	$7.4\cdot10^{-11}$	$2.0\cdot10^{-11}$
Phase 3							
1	999	700	200	$1.4\cdot10^{-17}$	$1.5\cdot10^{-17}$	$6.2\cdot10^{-11}$	$1.9\cdot10^{-11}$
1	999	601	200	$1.4\cdot10^{-17}$	$1.5\cdot10^{-17}$	$5.1\cdot10^{-11}$	$1.8\cdot10^{-11}$
1	999	501	200	$1.3\cdot10^{-17}$	$1.5\cdot10^{-17}$	$4.0\cdot10^{-11}$	$1.8\cdot10^{-11}$
3	999	401	200	$1.3\cdot10^{-17}$	$1.5\cdot10^{-17}$	$3.2\cdot10^{-11}$	$1.9\cdot10^{-11}$

Table XVII: Results of gas permeability measurements in sample 5 (test PG5_8) obtained with the steady-state method (ρ_d=2.32 g/cm^3, *w*=0.9%)

Duration (h)	Confining *P* (kPa)	Injection *P* (kPa)	Back *P* (kPa)	$k_{ig}\cdot k_{rg}$ inflow (m^2)	$k_{ig}\cdot k_{rg}$ outflow (m^2)	k_g inflow (m/s)	k_g outflow (m/s)
Phase 1							
1.3	1480	170	100	$4.4\cdot10^{-17}$	$4.8\cdot10^{-17}$	$4.7\cdot10^{-11}$	$2.9\cdot10^{-11}$
1.0	1490	220	100	$1.4\cdot10^{-17}$	$4.1\cdot10^{-17}$	$1.9\cdot10^{-11}$	$2.5\cdot10^{-11}$
3.3	1490	270	100	$2.4\cdot10^{-17}$	$3.6\cdot10^{-17}$	$4.0\cdot10^{-11}$	$2.2\cdot10^{-11}$
1.5	1490	320	100	$2.6\cdot10^{-17}$	$3.4\cdot10^{-17}$	$5.3\cdot10^{-11}$	$2.1\cdot10^{-11}$
16.5	1480	370	100	$2.9\cdot10^{-17}$	$3.1\cdot10^{-17}$	$6.7\cdot10^{-11}$	$1.9\cdot10^{-11}$
1.0	1470	420	100	$2.9\cdot10^{-17}$	$3.0\cdot10^{-17}$	$7.7\cdot10^{-11}$	$1.8\cdot10^{-11}$
3.7	1480	470	100	$2.9\cdot10^{-17}$	$2.9\cdot10^{-17}$	$8.5\cdot10^{-11}$	$1.7\cdot10^{-11}$
1.0	1480	520	100	$2.9\cdot10^{-17}$	$2.8\cdot10^{-17}$	$9.3\cdot10^{-11}$	$1.7\cdot10^{-11}$
18.8	1460	570	100	$2.9\cdot10^{-17}$	$2.7\cdot10^{-17}$	$1.0\cdot10^{-10}$	$1.6\cdot10^{-11}$
1.8	1470	620	100	$2.8\cdot10^{-17}$	$2.6\cdot10^{-17}$	$1.1\cdot10^{-10}$	$1.6\cdot10^{-11}$
2.7	1470	670	100	$2.7\cdot10^{-17}$	$2.5\cdot10^{-17}$	$1.1\cdot10^{-10}$	$1.5\cdot10^{-11}$
1.8	1480	720	100	$2.7\cdot10^{-17}$	$2.5\cdot10^{-17}$	$1.2\cdot10^{-10}$	$1.5\cdot10^{-11}$
1.0	1480	770	100	$2.8\cdot10^{-17}$	$2.5\cdot10^{-17}$	$1.3\cdot10^{-10}$	$1.6\cdot10^{-11}$
15.8	1460	820	100	$2.8\cdot10^{-17}$	$2.6\cdot10^{-17}$	$1.4\cdot10^{-10}$	$1.6\cdot10^{-11}$
2.0	1460	870	100	$2.9\cdot10^{-17}$	$2.6\cdot10^{-17}$	$1.5\cdot10^{-10}$	$1.6\cdot10^{-11}$
2.0	1470	920	100	$2.9\cdot10^{-17}$	$2.7\cdot10^{-17}$	$1.6\cdot10^{-10}$	$1.6\cdot10^{-11}$
1.3	1470	970	100	$2.9\cdot10^{-17}$	$2.8\cdot10^{-17}$	$1.7\cdot10^{-10}$	$1.7\cdot10^{-11}$

Duration (h)	Confining *P* (kPa)	Injection *P* (kPa)	Back *P* (kPa)	$k_{ig}{\cdot}k_{rg}$ inflow (m^2)	$k_{ig}{\cdot}k_{rg}$ outflow (m^2)	k_g inflow (m/s)	k_g outflow (m/s)
0.9	1470	920	100	$2.9{\cdot}10^{-17}$	$2.7{\cdot}10^{-17}$	$1.7{\cdot}10^{-10}$	$1.7{\cdot}10^{-11}$
0.8	1480	870	100	$2.8{\cdot}10^{-17}$	$2.6{\cdot}10^{-17}$	$1.5{\cdot}10^{-10}$	$1.6{\cdot}10^{-11}$
0.8	1480	820	100	$2.9{\cdot}10^{-17}$	$2.6{\cdot}10^{-17}$	$1.5{\cdot}10^{-10}$	$1.6{\cdot}10^{-11}$
14.5	1460	770	100	$2.8{\cdot}10^{-17}$	$2.5{\cdot}10^{-17}$	$1.3{\cdot}10^{-10}$	$1.5{\cdot}10^{-11}$
1.9	1460	720	100	$2.7{\cdot}10^{-17}$	$2.5{\cdot}10^{-17}$	$1.2{\cdot}10^{-10}$	$1.5{\cdot}10^{-11}$
0.7	1460	670	100	$2.7{\cdot}10^{-17}$	$2.5{\cdot}10^{-17}$	$1.1{\cdot}10^{-10}$	$1.5{\cdot}10^{-11}$
1.2	1460	620	100	$2.8{\cdot}10^{-17}$	$2.5{\cdot}10^{-17}$	$1.1{\cdot}10^{-10}$	$1.5{\cdot}10^{-11}$
1.0	1460	570	100	$2.8{\cdot}10^{-17}$	$2.6{\cdot}10^{-17}$	$1.0{\cdot}10^{-10}$	$1.6{\cdot}10^{-11}$
1.0	1460	520	100	$2.8{\cdot}10^{-17}$	$2.6{\cdot}10^{-17}$	$9.0{\cdot}10^{-11}$	$1.6{\cdot}10^{-11}$
3.3	1470	470	100	$2.8{\cdot}10^{-17}$	$2.7{\cdot}10^{-17}$	$8.1{\cdot}10^{-11}$	$1.7{\cdot}10^{-11}$
1.8	1470	420	100	$2.8{\cdot}10^{-17}$	$2.8{\cdot}10^{-17}$	$7.4{\cdot}10^{-11}$	$1.7{\cdot}10^{-11}$
61.1	1450	370	100	$2.9{\cdot}10^{-17}$	$2.9{\cdot}10^{-17}$	$6.6{\cdot}10^{-11}$	$1.8{\cdot}10^{-11}$
2.7	1450	320	100	$2.4{\cdot}10^{-17}$	$3.1{\cdot}10^{-17}$	$4.9{\cdot}10^{-11}$	$1.9{\cdot}10^{-11}$
2.2	1450	270	100	$3.6{\cdot}10^{-17}$	$3.4{\cdot}10^{-17}$	$6.1{\cdot}10^{-11}$	$2.1{\cdot}10^{-11}$
2.8	1450	220	100	$3.8{\cdot}10^{-17}$	$3.8{\cdot}10^{-17}$	$5.2{\cdot}10^{-11}$	$2.3{\cdot}10^{-11}$
18.0	1420	170	100	$4.2{\cdot}10^{-17}$	$4.5{\cdot}10^{-17}$	$4.5{\cdot}10^{-11}$	$2.8{\cdot}10^{-11}$
Phase 2							
1.6	590	170	100	$8.9{\cdot}10^{-17}$	$9.5{\cdot}10^{-17}$	$9.6{\cdot}10^{-11}$	$5.8{\cdot}10^{-11}$
1.7	890	470	100	$6.3{\cdot}10^{-17}$	$6.8{\cdot}10^{-17}$	$1.8{\cdot}10^{-10}$	$4.1{\cdot}10^{-11}$
1.6	1190	770	100	$5.5{\cdot}10^{-17}$	$5.4{\cdot}10^{-17}$	$2.6{\cdot}10^{-10}$	$3.3{\cdot}10^{-11}$
1.1	1490	1070	100	$4.9{\cdot}10^{-17}$	$4.8{\cdot}10^{-17}$	$3.3{\cdot}10^{-10}$	$2.9{\cdot}10^{-11}$
1.6	1490	770	100	$2.4{\cdot}10^{-17}$	$2.3{\cdot}10^{-17}$	$1.1{\cdot}10^{-10}$	$1.4{\cdot}10^{-11}$
0.5	1180	770	100	$5.6{\cdot}10^{-17}$	$5.4{\cdot}10^{-17}$	$2.7{\cdot}10^{-10}$	$3.3{\cdot}10^{-11}$
16.0	1180	470	100	$2.9{\cdot}10^{-17}$	$2.9{\cdot}10^{-17}$	$8.5{\cdot}10^{-11}$	$1.8{\cdot}10^{-11}$
0.8	880	470	100	$6.5{\cdot}10^{-17}$	$6.5{\cdot}10^{-17}$	$1.9{\cdot}10^{-10}$	$4.0{\cdot}10^{-11}$
23.5	890	170	100	$4.5{\cdot}10^{-17}$	$5.7{\cdot}10^{-17}$	$4.9{\cdot}10^{-11}$	$3.5{\cdot}10^{-11}$
6.3	590	170	100	$9.2{\cdot}10^{-17}$	$1.0{\cdot}10^{-16}$	$9.9{\cdot}10^{-11}$	$6.3{\cdot}10^{-11}$
18.8	610	80	100	$3.6{\cdot}10^{-18}$	$1.4{\cdot}10^{-16}$	$1.9{\cdot}10^{-12}$	$8.5{\cdot}10^{-11}$

Table XVIII: Results of gas permeability measurements in sample 7 (test PG7_3) obtained with the steady-state method (ρ_d=2.30 g/cm^3, *w*=1.2%)

Confining *P* (kPa)	Injection *P* (kPa)	Back *P* (kPa)	$k_{ig}\cdot k_{rg}$ inflow (m^2)	$k_{ig}\cdot k_{rg}$ outflow (m^2)	k_g inflow (m/s)	k_g outflow (m/s)
Phase 1						
600	400	90	$1.1\cdot10^{-16}$	$1.1\cdot10^{-16}$	$2.7\cdot10^{-10}$	$6.9\cdot10^{-11}$
700	500	90	$8.1\cdot10^{-17}$	$8.1\cdot10^{-17}$	$2.0\cdot10^{-10}$	$5.2\cdot10^{-11}$
800	600	90	$7.1\cdot10^{-17}$	$7.2\cdot10^{-17}$	$2.2\cdot10^{-10}$	$4.5\cdot10^{-11}$
900	700	90	$6.6\cdot10^{-17}$	$6.6\cdot10^{-17}$	$2.4\cdot10^{-10}$	$4.2\cdot10^{-11}$
1000	800	90	$6.0\cdot10^{-17}$	$6.0\cdot10^{-17}$	$2.6\cdot10^{-10}$	$3.8\cdot10^{-11}$
1100	900	90	$5.8\cdot10^{-17}$	$5.7\cdot10^{-17}$	$2.9\cdot10^{-10}$	$3.6\cdot10^{-11}$
1200	1000	90	$5.6\cdot10^{-17}$	$5.4\cdot10^{-17}$	$3.1\cdot10^{-10}$	$3.5\cdot10^{-11}$
1300	1100	90	$5.3\cdot10^{-17}$	$5.2\cdot10^{-17}$	$3.3\cdot10^{-10}$	$3.3\cdot10^{-11}$
Phase 2						
1400	1200	90	$5.0\cdot10^{-17}$	$4.8\cdot10^{-17}$	$3.7\cdot10^{-10}$	$3.0\cdot10^{-11}$
1400	1100	90	$4.8\cdot10^{-17}$	$4.6\cdot10^{-17}$	$3.2\cdot10^{-10}$	$2.9\cdot10^{-11}$
1400	1000	90	$4.5\cdot10^{-17}$	$4.4\cdot10^{-17}$	$2.8\cdot10^{-10}$	$2.8\cdot10^{-11}$
1400	900	90	$4.4\cdot10^{-17}$	$4.3\cdot10^{-17}$	$2.4\cdot10^{-10}$	$2.7\cdot10^{-11}$
1400	800	90	$4.4\cdot10^{-17}$	$4.2\cdot10^{-17}$	$2.2\cdot10^{-10}$	$2.7\cdot10^{-11}$
1480	700	90	$4.1\cdot10^{-17}$	$4.1\cdot10^{-17}$	$1.8\cdot10^{-10}$	$2.5\cdot10^{-11}$
1490	600	90	$4.3\cdot10^{-17}$	$4.2\cdot10^{-17}$	$1.6\cdot10^{-10}$	$2.5\cdot10^{-11}$
1490	500	90	$4.4\cdot10^{-17}$	$4.4\cdot10^{-17}$	$1.4\cdot10^{-10}$	$2.6\cdot10^{-11}$
1500	400	90	$4.9\cdot10^{-17}$	$4.6\cdot10^{-17}$	$1.2\cdot10^{-10}$	$2.8\cdot10^{-11}$
1530	300	90	$4.8\cdot10^{-17}$	$5.0\cdot10^{-17}$	$8.9\cdot10^{-11}$	$3.0\cdot10^{-11}$
1570	200	90	$5.0\cdot10^{-17}$	$5.8\cdot10^{-17}$	$6.3\cdot10^{-11}$	$3.5\cdot10^{-11}$
1600	150	90	$4.5\cdot10^{-17}$	$7.4\cdot10^{-17}$	$4.3\cdot10^{-11}$	$4.3\cdot10^{-11}$

Table XIX: Results of gas permeability measurements in sample 9 (test PG9_2) obtained with the steady-state method (ρ_d=2.32 g/cm^3, *w*=1.1%)

Duration (h)	Confining *P* (kPa)	Injection *P* (kPa)	Back *P* (kPa)	$k_{ig}\cdot k_{rg}$ inflow (m^2)	$k_{ig}\cdot k_{rg}$ outflow (m^2)	k_g inflow (m/s)	k_g outflow (m/s)
Phase 1							
1.8	1510	120	90	$1.6\cdot10^{-16}$	$7.2\cdot10^{-17}$	$1.1\cdot10^{-10}$	$4.4\cdot10^{-11}$
0.5	1510	150	100	$6.7\cdot10^{-16}$	$6.5\cdot10^{-16}$	$6.3\cdot10^{-10}$	$4.3\cdot10^{-10}$
2.6	1490	200	100	$7.5\cdot10^{-16}$	$6.8\cdot10^{-16}$	$9.2\cdot10^{-10}$	$4.4\cdot10^{-10}$
16.4	1490	250	100	$1.4\cdot10^{-16}$	$6.4\cdot10^{-16}$	$2.2\cdot10^{-10}$	$4.1\cdot10^{-10}$
1.1	1490	300	100	$1.0\cdot10^{-16}$	$6.5\cdot10^{-16}$	$1.9\cdot10^{-10}$	$4.3\cdot10^{-10}$
1.3	1490	350	100	$7.9\cdot10^{-17}$	$6.5\cdot10^{-16}$	$1.7\cdot10^{-10}$	$4.3\cdot10^{-10}$
0.8	1490	400	100	$6.6\cdot10^{-17}$	$6.7\cdot10^{-16}$	$1.6\cdot10^{-10}$	$4.4\cdot10^{-10}$
0.6	1490	450	100	$5.2\cdot10^{-17}$	$6.9\cdot10^{-16}$	$1.5\cdot10^{-10}$	$4.5\cdot10^{-10}$
1.6	1490	500	100	$4.5\cdot10^{-17}$	$7.0\cdot10^{-16}$	$1.4\cdot10^{-10}$	$4.7\cdot10^{-10}$
0.8	1490	550	100	$3.8\cdot10^{-17}$	$7.1\cdot10^{-16}$	$1.3\cdot10^{-10}$	$4.7\cdot10^{-10}$
2.4	1500	600	100	$3.4\cdot10^{-17}$	$7.2\cdot10^{-16}$	$1.3\cdot10^{-10}$	$4.8\cdot10^{-10}$
Phase 2							
17.0	1210	600	100	$9.0\cdot10^{-16}$	$9.0\cdot10^{-16}$	$3.4\cdot10^{-9}$	$6.1\cdot10^{-10}$
1.5	1210	300	100	$1.7\cdot10^{-16}$	$9.9\cdot10^{-16}$	$3.2\cdot10^{-10}$	$6.6\cdot10^{-10}$
4.1	910	300	100	$1.8\cdot10^{-16}$	$1.5\cdot10^{-15}$	$3.4\cdot10^{-10}$	$1.0\cdot10^{-9}$
1.9	710	300	100	$1.9\cdot10^{-16}$	$2.1\cdot10^{-15}$	$3.6\cdot10^{-10}$	$1.4\cdot10^{-9}$
17.4	710	200	100	$5.5\cdot10^{-16}$	$2.2\cdot10^{-15}$	$6.8\cdot10^{-10}$	$1.5\cdot10^{-9}$
4.9	510	200	100	$5.8\cdot10^{-16}$	$3.2\cdot10^{-15}$	$7.2\cdot10^{-10}$	$2.1\cdot10^{-9}$

Table XX: Results of gas permeability measurements in sample 10 (test PG10_1) obtained with the steady-state method (ρ_d=2.28 g/cm^3, *w*=4.0%)

Duration (h)	Confining *P* (kPa)	Injection *P* (kPa)	Back *P* (kPa)	$k_{ig}\cdot k_{rg}$ inflow (m^2)	$k_{ig}\cdot k_{rg}$ outflow (m^2)	k_g inflow (m/s)	k_g outflow (m/s)
1.5	1500	120	100	$5.4\cdot10^{-16}$	$1.4\cdot10^{-16}$	$3.7\cdot10^{-10}$	$8.6\cdot10^{-11}$
1.1	1490	170	100	$6.5\cdot10^{-16}$	$7.0\cdot10^{-16}$	$6.1\cdot10^{-10}$	$4.7\cdot10^{-10}$
2.1	1480	220	100	$5.5\cdot10^{-16}$	$5.5\cdot10^{-16}$	$6.9\cdot10^{-10}$	$3.7\cdot10^{-10}$
1.8	1480	270	100	$4.4\cdot10^{-16}$	$4.4\cdot10^{-16}$	$6.9\cdot10^{-10}$	$3.0\cdot10^{-10}$
1.8	1480	320	100	$3.7\cdot10^{-16}$	$3.7\cdot10^{-16}$	$7.0\cdot10^{-10}$	$2.5\cdot10^{-10}$
21.8	1440	370	100	$3.1\cdot10^{-16}$	$3.0\cdot10^{-16}$	$6.7\cdot10^{-10}$	$2.1\cdot10^{-10}$

DATA OF MEASUREMENTS OF WATER PERMEABILITY

Table XXI: Values of hydraulic conductivity obtained in the concrete samples used for the gas permeability tests after saturation with deionised water

Ref [a]	ρ_d inicial (g/cm^3)	Initial w (%)	Initial S_r (%)	Time [b] (days)	k_w (m/s)	k_{iw} (m^2)	Final w (%)	Final S_r (%)	T (°C)
HOR0	2.26	4.8	68	40	$4.1\cdot10^{-11}$	$4.2\cdot10^{-18}$	6.2	91	22
HOR4	2.30	2.6	42	19	$1.1\cdot10^{-7}$	$1.1\cdot10^{-14}$	4.0	65	24
HOR4s	2.33	1.5	28	17	$2.0\cdot10^{-10}$	$2.0\cdot10^{-17}$	4.9	89	22
HOR3	2.36	1.9	36	16	$6.3\cdot10^{-11}$	$6.4\cdot10^{-18}$	3.7	72	26
HOR3s	2.36	1.2	23	246	$6.5\cdot10^{-12}$	$6.6\cdot10^{-19}$	4.6	94	23
HOR6s	2.32	0.0	0	50	$4.1\cdot10^{-9}$	$4.1\cdot10^{-16}$	4.1	71	22
HOR6s_2	2.31	0.9	15	51	$4.0\cdot10^{-11}$	$4.0\cdot10^{-18}$	4.9	82	20
HOR6s_3	2.30	1.1	18	86	$4.7\cdot10^{-11}$	$4.8\cdot10^{-18}$	5.0	87	22
HOR5	2.32	0.8	14	23	$1.9\cdot10^{-11}$	$1.9\cdot10^{-18}$	4.3	74	23
HOR5s	2.32	4.0	69	18	$4.5\cdot10^{-11}$	$4.6\cdot10^{-18}$	4.8	82	21
HOR5s_2	2.32	0.9	15	66	$1.5\cdot10^{-11}$	$1.6\cdot10^{-18}$	5.0	97	19
HOR2s	2.32	0.9	15	5	$1.9\cdot10^{-9}$	$1.9\cdot10^{-16}$	4.7	81	24
HOR1s	2.37	0.7	11	356	$1.3\cdot10^{-11}$	$1.3\cdot10^{-18}$	4.6	95	20
HOR1s_2	2.37	1.2	23	43	$7.7\cdot10^{-12}$	$7.9\cdot10^{-19}$	4.7	92	21
HOR7s	2.30	1.1	18	23	$1.8\cdot10^{-11}$	$1.9\cdot10^{-18}$	5.4	87	22
HOR7s_2	2.30	1.2	19	123	$6.3\cdot10^{-12}$	$6.4\cdot10^{-19}$	5.7	94	23
HOR9s	2.32	0.8	14	101	$4.5\cdot10^{-12}$	$4.6\cdot10^{-19}$	5.2	92	23
HOR10s	2.24	1.7	23	121	$2.0\cdot10^{-11}$	$2.1\cdot10^{-18}$	5.9	95	21

[a] An s in the reference indicates that the sample was previously air dried

[b] Time needed to get a stable permeability value. In the case of values <50 it indicates the time the measurement was performed, although it was not an equilibrium value

1135-9420